JIPB Journal of Integrative Plant Biology

Research Article
https://doi.org/10.1111/jipb.70196

Tandemly duplicated *TaERF109* genes confer drought tolerance and post-drought recovery in wheat

Jun Chen[1†], Shang Zhao[1†], Wenjing Li[1†], Chunxiao Wang[2†], Yuan Gao[1], Zihan Yang[1], Yongbin Zhou[1], Ming Chen[1], Zhaoshi Xu[1] and Youzhi Ma[1*]

1. State Key Laboratory of Crop Gene Resources and Breeding, Institute of Crop Sciences, Chinese Academy of Agricultural Sciences (CAAS), Beijing 100081, China
2. Northwest Agricultural and Forestry University, Yangling 712100, China
†These authors contributed equally to this work.
*Correspondence: Youzhi Ma (mayouzhi@caas.cn)

Jun Chen

Youzhi Ma

ABSTRACT

To adapt to environmental challenges, plants have evolved extensive gene families through duplication events, generating multiple-copy genes that mediate stress responses. However, the function of these duplicated genes in wheat remains unclear. In this study, we identified ten tandemly duplicated *ETHYLENE RESPONSE FACTOR 109* (*ERF109*) genes in wheat, seven of which showed rapid induction under drought treatment. Overexpressing *TaERF109A2* resulted in delayed heading date, increased tiller number, reduced plant height and root length, and enhanced drought resilience. Conversely, the CRISPR/Cas9-generated nonuple *Taerf109s* mutant showed exacerbated growth inhibition under drought stress. RNA-seq and functional analyses indicated that *TaMADS56*, functioning as a genetic downstream effector of *TaERF109A2*, modulates wheat tillering, heading date, and drought recovery responses. TaERF109A2 directly binds to the GCC-box motifs in the promoters of *TaIPT8-5B/5D*, thereby regulating cytokinin (CK) biosynthesis. Moreover, overexpression of *TaERF109A2* enhances nicotianamine (NA) accumulation, which in turn confers tolerance to iron toxicity and drought stress via upregulation of nicotianamine synthase (*NAS*) genes. Our findings have highlighted the critical role of tandemly duplicated genes in the coordination of stress responses and developmental processes in wheat.

Keywords: drought tolerance, ERF109, tandemly duplicated genes, wheat

Chen, J., Zhao, S., Li, W., Wang, C., Gao, Y., Yang, Z., Zhou, Y., Chen, M., Xu, Z., and Ma, Y. (2026). Tandemly duplicated *TaERF109* genes confer drought tolerance and post-drought recovery in wheat. J. Integr. Plant Biol. **68:** 1744–1761.

INTRODUCTION

As one of the world's key staple crops, wheat is predominantly grown in arid and semi-arid regions, where drought is the primary abiotic constraint limiting grain yield (Hussain et al., 2018). Elucidating the molecular mechanisms underlying plant responses to water deficit stress is critical for enhancing wheat adaptation and maintaining yield stability under climate change.

To mitigate drought-induced damage, plants initiate coordinated physiological and biochemical adaptations, including stomatal closure, growth retardation, photosynthetic

downregulation, and increased biosynthesis of osmolytes, antioxidants, and molecular chaperones (Reddy et al., 2004; Yang and Qin, 2023). These adaptive responses are usually mediated by plant hormones and signaling molecules, such as abscisic acid (ABA). This has long been recognized as the primary stress-induced hormone that mediates ROS generation and stomatal closure (Pei et al., 2000; Li et al., 2017a). Extensive attention has been paid to the role of CK in abiotic stress responses. Here, endogenous CK levels are dynamically regulated through transcriptional modulation of CK biosynthesis and degradation genes (Prerostova et al., 2018). In wheat, soybean, cabbage, and apple, several abiotic-responsive *ISOPENTENYLTRANSFERASE* (*IPT*) genes are rapidly induced before returning to pretreatment levels under sustained moderate stress. A few are maintained at high expression levels when challenged with severe stress conditions (Nishiyama et al., 2011; Le et al., 2012; Liu et al., 2013; Tan et al., 2018). Achieved by transgenic plants overexpressing an *IPT* gene through senescence- or stress-induced promoters, CK elevation improves drought tolerance by enhancing photosynthetic protection, delaying senescence, and increasing redox potential (Rivero et al., 2007; Ma and Liu, 2009; Zhang et al., 2010; Merewitz et al., 2011; Peleg et al., 2011; Qin et al., 2011). In contrast, CK downregulation achieved by the constitutive overexpression of cytokinin oxidase/dehydrogenase (*CKX*) genes or the knockout of *IPT* genes may also have a positive effect on drought tolerance (Nishiyama et al., 2011; Werner et al., 2011; Macková et al., 2013). These transformants may have substantially altered phenotypes, such as enhanced root systems, dwarf shoots, slow growth rates, and smaller leaves, which minimize water loss (Werner et al., 2011). A recent study on the wheat drought-induced *IPT* gene *TaIPT8* showed that CK deficiency in *TaIPT8-5A/5B/5D* triple mutants significantly impaired drought tolerance without affecting normal growth, highlighting the positive role of CKs in wheat drought resilience (Wang et al., 2023).

Although drought-induced physiological and biochemical responses have been extensively examined in crops, our understanding of the molecular mechanisms influencing post-drought recovery remains limited (Abid et al., 2018). Unlike drought avoidance strategies such as leaf area reduction and stomatal closure, which conserve water, post-drought recovery involves relieving photosynthetic limitations, including leaf rehydration, stomatal reopening for CO_2 assimilation, and *de novo* synthesis of photosynthetic machinery (KIRSCHBAUM, 1988). Transcriptomic studies have shown that photosynthesis-related genes are dynamically upregulated during water recovery from drought stress (Zhang et al., 2018). MADS-box transcription factors play vital roles in the regulation of photosynthesis and stomatal movement (Hoenicka et al., 2008; Matsubara et al., 2008; Li et al., 2017b). In *Arabidopsis thaliana*, the MADS-box genes *SUPPRESSOR OF OVEREXPRESSION OF CO1* (*SOC1*) and *AGAMOUS-like 16* (*AGL16*) are partly expressed in mature guard cells and are involved in the positive regulation of stomatal density and opening (Kutter et al., 2007; Kimura et al., 2015). *SOC1*-like genes function as floral integrators and promote vegetative growth (Borner et al., 2000; Melzer et al., 2008; Lee and Lee, 2010). An ortholog of *SOC1* in rice, *OsMADS50,* activates drought escape responses by upregulating the flowering-promoting genes *OsMADS14/15/18* independently of ABA signaling (Jin et al., 2013). However, the role of *SOC1* homologs in wheat drought tolerance and recovery remains unclear.

Gene duplication is an important factor in species adaptation, diversity, and speciation (Flagel and Wendel, 2009; Glover et al., 2015). These duplication events involve the whole genome, large-scale segments, and small-scale segments in which only one or a few genes are duplicated (Panchy et al., 2016). Tandem duplication refers to the generation of tandem arrays consisting of identical genes close to each other on the same chromosome, and occurs due to unequal chromosomal crossing accompanied by inversion events (Kane et al., 2010). The lineage-specific expansion of tandem duplicates in plants often confers adaptive advantages to environmental responses (Hanada et al., 2008). Recent genomic studies have suggested that the Triticeae lineage, particularly wheat, has undergone accelerated evolution via frequent gene duplication and rearrangement characterized by high rates of inversions and translocations (Glover et al., 2015).

The APETALA2/ethylene-responsive (AP2/ERF) superfamily is one of the largest groups of plant-specific transcription factors known for their regulatory roles in plant developmental processes and biotic/abiotic stress responses (Xu et al., 2011; Cai et al., 2014; Jung et al., 2017). The AP2/ERF genes can be classified into four major subfamilies, namely, AP2, ERF, DREB, and RAV, based on the presence and specificity of their domains (Sakuma et al., 2002; Nakano et al., 2006). In wheat, *TaERF* and *TaDREB* subfamilies show gene family expansion driven by intronless tandem duplications, in contrast to the conserved *TaAP2* subfamily (Magar et al., 2022). However, the hexaploid nature of common wheat makes understanding the precise molecular functions of these duplicated genes, which usually have three homologs located in each of the three subgenomes, very challenging.

In this study, we identified 10 *TaERF109* genes that are tandemly distributed in the wheat genome. We confirmed their positive role in drought stress and rehydration by overexpressing *TaERF109A2* and constructing a nonuple *Taerf109s* mutant carrying mutations in nine members of the *TaERF109s* in cv. Fielder. Functional analyses showed that TaERF109A2 acts upstream of TaMADS56 to inhibit the heading date while promoting tiller outgrowth and drought recovery. TaERF109A2 directly binds to GCC-box motifs in *TaIPT8-5B/5D* promoters to activate CK biosynthesis and indirectly upregulates *NAS* genes. This enhances NA accumulation and iron tolerance. These findings establish TaERF109 as a key node that integrates developmental processes with CK and NA biosynthesis in wheat drought and rehydration responses.

RESULTS

TaERF109s are tandemly duplicated genes highly responsive to drought

To identify drought-responsive tandemly duplicated genes (TDGs) and elucidate the molecular mechanisms underlying drought adaptation in wheat, we performed a comparative transcriptome analysis of wheat plants subjected to drought stress and well-watered control conditions. Among the 14,784 differentially expressed genes (DEGs) identified, 1,210 were classified as TDGs (Data S1). By leveraging fold-change thresholds and false discovery rate (FDR) corrections, we prioritized 10 candidate genes encoding putative ERF109-like transcription factors for in-depth functional validation (Table S1). Genome-wide sequence analysis of the "Chinese Spring" cultivar was used to identify 10 *TaERF109* homeologs distributed across three subgenomes, that is, three TDGs (TraesCS1A02G370400, TraesCS1A02G370600, TraesCS1A02G370700) on Chromosome 1A, three TDGs (TraesCS1B02G389700, TraesCS1B02G389800, TraesCS1B02G389900) on Chromosome 1B, and four TDGs (TraesCS1D02G376500, TraesCS1D02G376600, TraesCS1D02G376700, TraesCS1D02G376800) on Chromosome 1D (Figure 1A). These were designated *TaERF109A1–A3*, *TaERF109B1–B3*, and *TaERF109D1–D4*, respectively. *TaERF109B2* was absent in the "Fielder" cultivar, as revealed by polymerase chain reaction (PCR) amplification failure and basic local alignment search tool (BLAST) analysis of the "Fielder" genome assembly (Sato et al., 2021), which contained only nine *TaERF109* homologs (Figure 1A). To assess copy number variation at the *TaERF109* locus, we screened the publicly available genomic variation data from 145 landmark

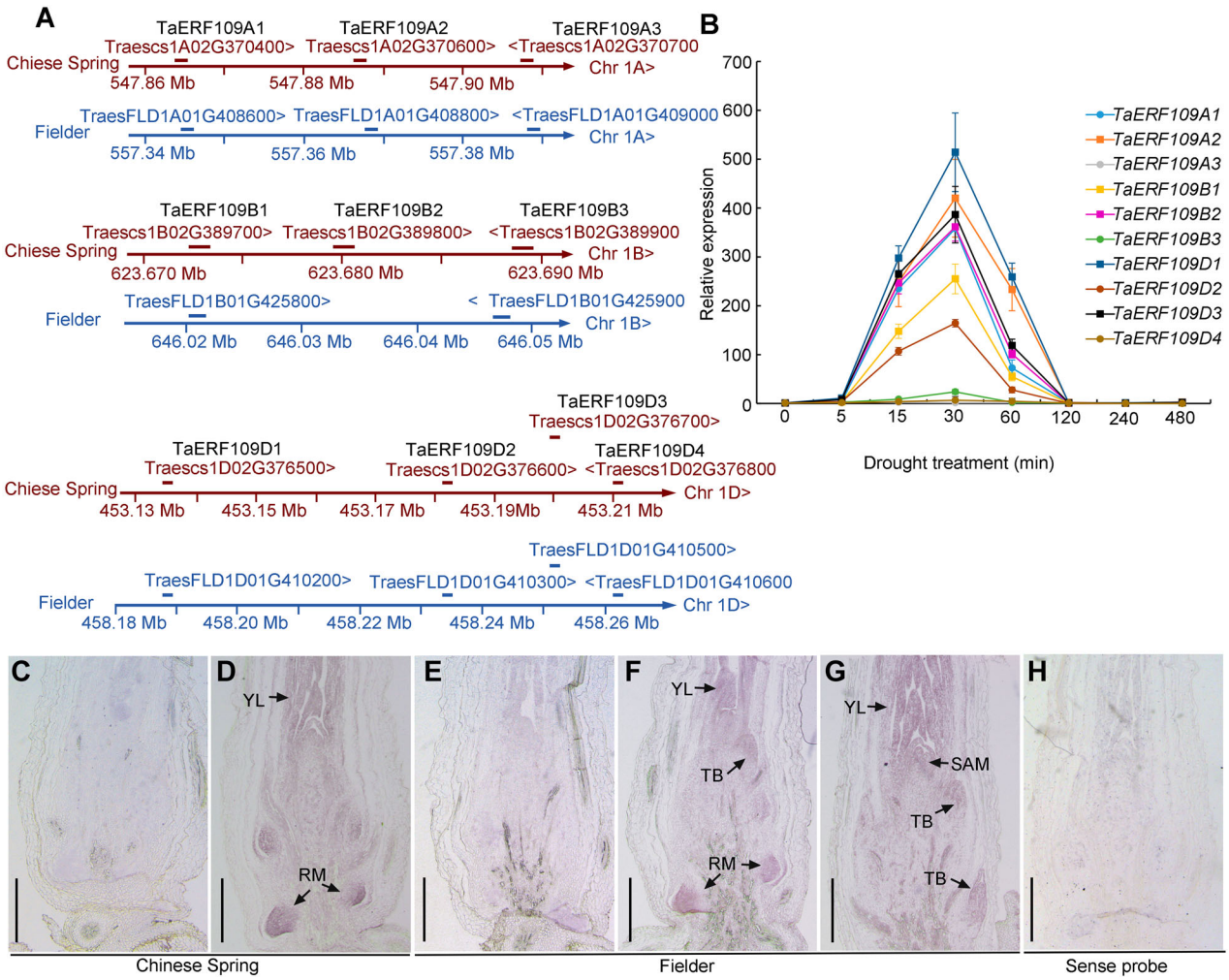

Figure 1. Genomic location and expression pattern of *TaERF109* homologs in wheat

(A) The genomic location of *TaERF109* homologs across the A, B, and D subgenomes of hexaploid wheat. **(B)** Expression patterns of *TaERF109* homologs in Chinese Spring under drought stress. Y-axes represent fold changes relative to the unstressed control, and x-axes denote treatment time points at 0, 5, 15, 30, 60, 120, 240, and 480 min. The *TaActin* gene was used as an internal reference. The data represent the means ± *SD* of three independent biological replicates. **(C–G)** RNA *in situ* hybridization showed preferential expression of *TaERF109A2* in young leaves (YL), tiller buds (TB), root meristems (RM), and shoot apical meristems (SAM) before **(C, E)** and following 30 min drought treatment **(D, F,** and **G)**. Arrows highlight specific sites of *TaERF109A2* transcript accumulation. **(H)** The *TaERF109A2* sense probe was used as a negative control. Scale bars = 1 mm **(C–H)**.

cultivars (Hao et al., 2020; Wang et al., 2020). Genotypic data for the region encompassing *TaERF109B2* was completely missing in 11 of these 145 accessions, whereas no such absence was observed for other *TaERF109* homologs (Figure S1; Data S2). These results indicate that the deletion of *TaERF109B2* contributes to the copy number variation of *TaERF109* genes, which range from 9 to 10 copies in different hexaploid wheat accessions.

Protein domain analysis revealed that all 10 TaERF109 proteins harbor a single conserved AP2 domain (Figure S2A). Meanwhile, promoter sequence analysis identified diverse stress- and hormone-responsive cis-acting elements within their respective promoter regions (Figure S2B). To investigate whether *TaERF109s* are responsive to drought, other abiotic stresses, and plant hormones, real-time quantitative polymerase chain reaction (RT-qPCR) analyses were performed using specific primers for the 10 *TaERF109s* in "Chinese Spring". Transcription of *TaERF109A1*, *TaERF109A2*, *TaERF109B1*, *TaERF109B2*, *TaERF109D1*, *TaERF109D2*, and *TaERF109D3* was strongly induced after 5 min of drought treatment. This reached peak induction levels of 200- to 500-fold 30 min before returning to basal levels (Figure 1B). The drought-responsive *TaERF109s* also displayed rapid transcriptional activation in response to cytokinin 6-benzylaminopurine (6-BA) treatment (Figure S3A). *TaERF109A2*, *TaERF109B1*, and *TaERF109B2* transcripts were significantly upregulated after 4 h of heat stress (Figure S3B). Meanwhile, *TaERF109A2* responded rapidly to NaCl treatment with a transient 30 min induction (Figure S3C). Minimal changes in expression were observed following auxin (IAA), methyl jasmonate (MeJA), and ABA treatments (Figure S3D–F). Under normal conditions, *TaERF109s* exhibit relatively low expression levels across various tissues without tissue specificity (Figure S4). Consistent with the RT-qPCR results, RNA in situ hybridization analysis further confirmed the drought-responsive expression of *TaERF109A2* in tissues with high cell proliferation activity, including young leaves, shoot apical meristems, tiller buds, and root meristems, following drought stress (Figure 1C–H).

TaERF109 contains a single AP2 domain near its C-terminal region. To assess their transcriptional activation potential, full-length *TaERF109A2* and its N/C-terminal truncations were fused to the GAL4 DNA-binding domain and expressed in the yeast strain Y2HGold (Figure S5A). Both full-length TaERF109A2 and the C-terminal fragment containing the AP2 domain activated the reporter gene expression, confirming their transcriptional activation activity (Figure S5B). Subcellular localization studies were performed by generating a *TaERF109A2-GFP* fusion construct that was transiently expressed in wheat leaf protoplasts. Confocal microscopy showed the exclusive co-localization of TaERF109A2-GFP with the nuclear marker Early heading date 4 (EHD4)-mCherry (Figure S5C–F), indicating that TaERF109A2 functioned in the nucleus. These results support the notion that TaERF109A2 is a nuclear-localized protein that likely functions as a transcriptional activator.

Tandem gene duplication events of *ERF109* may have occurred during Triticeae diversification

Genome scanning and phylogenetic analyses showed two orthologous *ERF109* loci in barley (*Hordeum vulgare*) and four orthologous loci in *Aegilops tauschii*, all organized in tandem arrays. In contrast, single-copy *ERF109* orthologs have been identified in other monocotyledonous species, including *Oryza sativa*, *Zea mays*, *Sorghum bicolor*, *Setaria italica*, and *Brachypodium distachyon* (Figure S6). Phylogenetic classification of the ten hexaploid wheat *TaERF109s* resolved two major clades. Group I contained seven *TaERF109s* (*TaERF109A1–A2*, *TaERF109B1–B2*, *TaERF109D1–D3*), and Group II contained three *TaERF109s* (*TaERF109A3*, *TaERF109B3*, *TaERF109D4*). All drought-responsive members identified through expression profiling clustered within Group I and were further subdivided into small subgroups. To further trace the evolutionary history of tandemly duplicated *TaERF109* homologs, we performed microcollinearity analysis of the genomic segments containing *ERF109* homologous copies using Triticeae-GeneTribe (Chen et al., 2020). Collinear blocks containing 2 to 6 tandemly duplicated *ERF109* genes were identified in the genomes of bread wheat and 11 other Triticeae species (Figure S7). In contrast, no such collinear blocks were detected in *B. distachyon*, *Oryza sativa Japonica*, *S. bicolor*, or *Z. mays*. These copy number variations and chromosomal distributions suggest that *ERF109* clusters formed by tandem duplication events are specific to the Triticeae lineage.

Overexpression of *TaERF109A2* has a pleiotropic effect on complex agronomic traits

To determine the biological functions of TaERF109s, we generated transgenic wheat lines overexpressing drought-responsive *TaERF109A2* and drought-unresponsive *TaERF109D4* under the control of the ubiquitin promoter in the spring wheat cultivar, "Fielder". Molecular characterization was used to identify nine independent *TaERF109A2*-overexpressing (OE) lines and two *TaERF109D4*-OE lines, showing over 1,000-fold induction compared to the negative control plants due to the low basal expression of these genes (Figure S8A, B). Constitutive expression of both genes induces dramatic pleiotropic effects on plant architecture and reproductive development (Figure 2A, B). At the seedling stage, the three homozygous T_3 *TaERF109A2*-OE lines displayed stunted shoot and root growth, accompanied by accelerated tiller bud outgrowth (Figure S8C–G). During the heading stage, *TaERF109A2*-OE lines exhibited > 20-d delayed heading, significantly increased tiller number, and shortened and thinner leaves compared to controls (Figure 2A, C). Mature plants showed a prostrate growth habit with reduced plant height, smaller spikes, and > 4-fold increase in tiller numbers (Figures 2D, E, S8H–J). Concomitantly, *TaERF109A2*-OE lines had severe reproductive defects, including extremely low seed-setting rates and inhibited grain filling, producing shriveled kernels (Figure S8K–N). The overexpression of *TaERF109D4* resulted in complete sterility, with no viable seeds produced (Figure S8O).

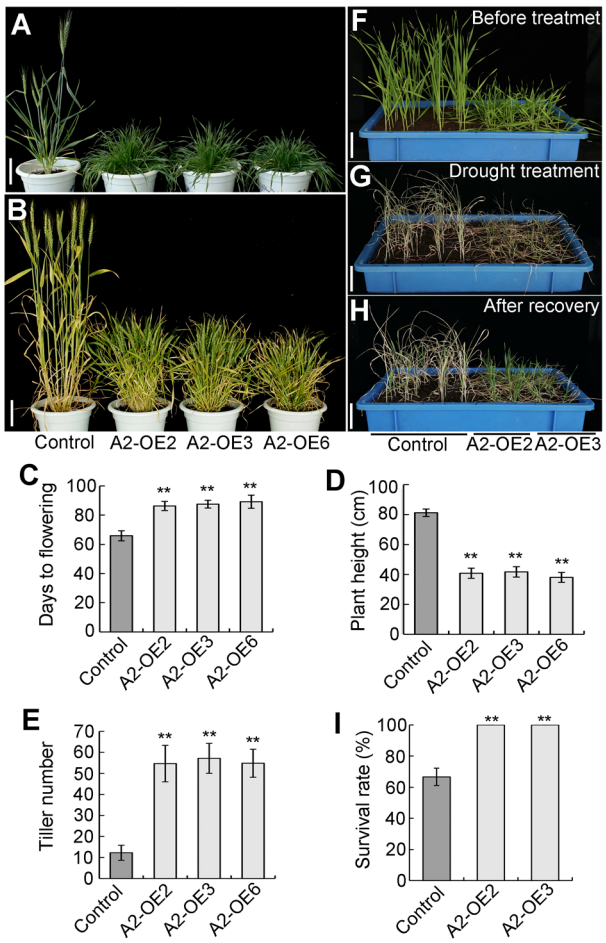

Figure 2. Phenotypic characterization of the *TaERF109A2*-OE plants

(A, B) Comparison of *TaERF109A2*-OE (A2-OE2, A2-OE3, and A2-OE6) and negative control plant at the tillering stage **(A)** and grain-filling stage **(B)**. Scale bar = 10 cm. In **(B)**, control plants were sown 20 d later than *TaERF109A2*-OE plants to synchronize developmental stages. **(C–E)** Comparison of flowering time **(C)**, plant height **(D),** and tiller number **(E)** between control and *TaERF109A2*-OE plants. **(F–H)** Physiological responses of seedlings affected by drought treatments and the water recovery period. Scale bar = 8 cm. **(I)** Statistical analysis of seedling survival rate between control and *TaERF109A2*-OE plants. Data are shown as means ± *SD* from three independent replicates. Significant differences were determined by a two-tailed Student's *t*-test (**$P < 0.01$).

TaERF109s positively regulate drought tolerance and post-drought recovery in wheat

Drought assays were conducted using shallow containers to evaluate drought resilience independent of the root architecture. While both *TaERF109A2*-OE and control plants exhibited severe wilting under dehydration, OE lines recovered rapidly with enhanced tillering and leaf regrowth after rehydration (Figure 2F–H) and showed higher survival rates than control plants (Figure 2I). Biochemical analyses further revealed that in *TaERF109A2*-OE plants, the proline content was significantly increased both before and after drought treatment, while the contents of malondialdehyde (MDA), hydrogen peroxide (H_2O_2), and superoxide (O_2^-) were significantly decreased after drought treatment (Figure S9). To validate the stress-regulatory roles of the *TaERF109* gene family, CRISPR/Cas9-mediated genome editing was performed using two guide RNAs targeting 23-bp spaced sites within the conserved AP2 domains of *TaERF109* loci (Figure S10A). After DNA sequencing with nine *TaERF109* gene-specific PCR primers, we isolated a homozygous *Taerf109s* nonuple mutant with 1–43 bp deletions in all *TaERF109* homeologs (Figure S10B). Under normal growth conditions, there were no significant differences in vegetative and reproductive growth between the *Taerf109s* mutant and wild-type (WT) plants (Figures 3A, S10C–L). However, drought stress exacerbated the growth inhibition and accelerated leaf rolling in the *Taerf109s* mutant (Figure 3B). Two weeks after rewatering, WT plants fully recovered. Meanwhile, *Taerf109s* mutants continued to wilt with significantly reduced fresh and dry weights (Figure 3C–E). Biochemical analyses showed that drought-stressed *Taerf109s* accumulated higher MDA, H_2O_2, and O_2^- levels but a lower proline content, compared with WT plants (Figure S11A–D). Under field drought conditions, *Taerf109s* exhibited a slight reduction in tiller number, along with significant decreases in the number of fertile florets per spike, grain number per spike, and 1,000-grain weight compared to WT (Figure 3F–L).

TaMADS56s act as downstream effectors of TaERF109A2 to regulate vegetative growth and post-drought recovery in wheat

To dissect the regulatory mechanisms underlying TaERF109A2-mediated morphological changes and drought resilience, RNA sequencing (RNA-seq) was performed on six-week-old young leaves from control and *TaERF109A2*-overexpressing seedlings. We identified 8,942 DEGs, comprising 4,607 upregulated and 4,335 downregulated genes. Among the most significantly upregulated genes (Log_2(fold change) >10) was *TaMADS56-7D*, an ortholog of the heading date regulator *SOC1* in *Arabidopsis* (Table S2). Two other *TaMADS56* homologous genes were also upregulated. Meanwhile, one *MADS18* homolog, one *MADS15* homolog, and two wheat *FLOWERING LOCUS T (FT)* genes (*TaFT1*/*TaFT2*) were strongly repressed (Table S2). RT-qPCR validation confirmed the RNA-seq results, showing 1,195-fold and 207-fold induction of *TaMADS56-7D* and *TaMADS56-7A*, respectively, and 592-fold and 145-fold repression of *TaFT1* and *TaFT2* in *TaERF109A2*-OE plants compared to the controls (Figure 4A–D).

Given the conserved roles of *SOC1*-like genes in coordinating vegetative development and flowering time across plant taxa, we hypothesized that *TaMADS56s* act as a downstream effector of TaERF109A2 in the regulation of wheat heading date and shoot architecture. To test this hypothesis, we generated transgenic wheat lines overexpressing *TaMADS56-7D* in "Fielder". Molecular characterization was used to identify seven independent *TaMADS56-7D*-overexpressing (56-OE) lines. Three of these were selected for detailed analysis based on their expression

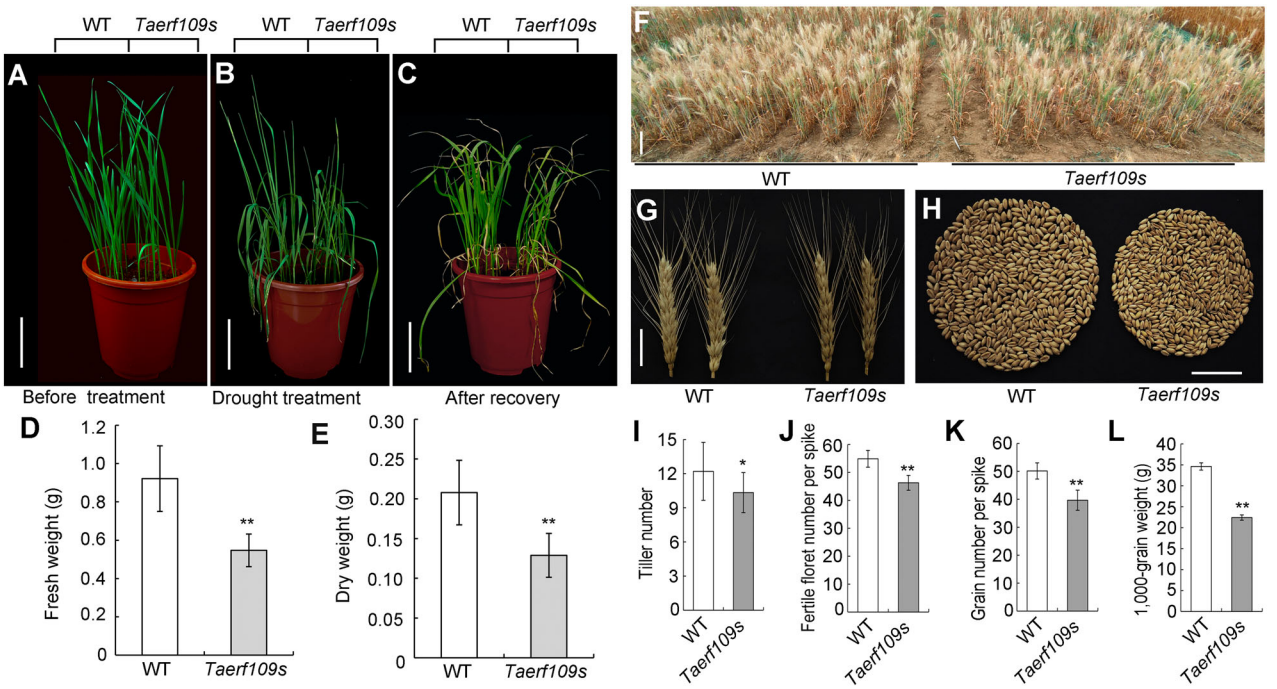

Figure 3. Drought tolerance phenotypes of *Taerf109s* mutant

(A–C) Phenotypes of *Taerf109s* and WT plants under normal growth and drought conditions. **(D, E)** Fresh weight **(D)** and dry weight **(E)** of *Taerf109s* and WT plants after water recovery. Data are shown as means ± *SD* from three independent replicates ($n = 9$). Significant differences were determined by a two-tailed Student's *t*-test (**$P < 0.01$). **(F–H)** Plant architecture **(F)**, spikes **(G),** and 500 seeds **(H)** of WT and *Taerf109s* plants under drought conditions in the field. **(I–L)** Tiller number **(I)**, fertile floret number per spike **(J)**, grain number per spike **(K)**, and 1,000-grain weight **(L)** of WT and *Taerf109s* plants under drought stress in the field. Data are shown as means ± *SD* ($n = 12$). Significant differences were determined by two-tailed Student's *t*-test ($0.01 < *P < 0.05$, **$P < 0.01$). Scale bar = 10 cm **(A–C)**, 20 cm **(F)**, 3 cm **(G),** and 4 cm **(H)**.

levels (Figure S12A). Phenotypic analysis showed the dose-dependent effects of *TaMADS56-7D* overexpression on developmental processes (Figure 4E, F). Under controlled long-day (LD, 14 h light/10 h dark) and natural long-day (NLD) conditions, 56-OE1 (40-fold induction) delayed heading by 2 d (LD) and 5 d (NLD). Meanwhile, 56-OE2 (196-fold) and 56-OE4 (164-fold) exhibited 8.5/13.7 d (LD/NLD) and 7/12 d (LD/NLD) delays, respectively (Figure 4G). The tiller number showed more pronounced responses, increasing by 47.9%–81.9% (LD) and 44.3%–109.4% (NLD) across all 56-OE lines (Figure 4H). Although plant height, grains per spike, and 1,000-grain weight decreased in OE plants, the yield outcomes diverged based on the expression levels (Figure 4I–K). 56-OE1 achieved a 16.70% yield increase compared to the control due to compensatory tillering (Figure 4L). Meanwhile, 56-OE2 and 56-OE4 showed yield parity with the controls despite extreme tiller proliferation, likely due to severely reduced grain number and size (Figure S12B). No significant differences in root architecture were observed between 56-OE lines and controls (Figure S12C–F).

As *TaMADS56* genes showed no transcriptional activation in yeast (Figure S13), we propose that they function as transcriptional repressors that negatively regulate *TaMADS18*, *TaMADS15*, and *TaFT* expression in wheat. To determine this, the transcript levels of these genes were evaluated using RT-qPCR 15 and 50 d after germination (DAG). At the seedling stage (15 DAG), all the detected genes showed low basal expression in both *TaMADS56*-OE and control plants. During the reproductive transition stage (50 DAG), the expression levels of the detected genes significantly increased in control plants and were significantly higher than those in *TaMADS56*-OE plants (Figure S14A–D). This has demonstrated that TaMADS56 acts upstream of *TaMADS15*, *TaMADS18*, and two *TaFT* in wheat heading regulation.

The enhanced vegetative growth observed in *TaMADS56*-OE plants prompted us to investigate whether *TaMADS56* positively affects drought stress tolerance. We evaluated the drought tolerance of *TaMADS56*-OE and control plants during vegetative growth. After withholding water for two weeks, similar drought symptoms, such as leaf rolling and wilting, appeared in both *TaMADS56*-OE lines and control plants. However, after two weeks of rewatering, the 56-OE2 and 56-OE4 plants recovered more rapidly from water stress, exhibiting significantly higher fresh and dry weights compared to controls (Figures 4M–O, S15). These findings suggest that *TaERF109s* modulate vegetative growth and post-drought recovery in wheat via TaMADS56-mediated pathways.

TaERF109A2 directly activates *TaIPT8* to promote CK biosynthesis in wheat

To elucidate the molecular mechanisms by which TaERF109s regulate root morphology, Kyoto Encyclopedia of Genes and

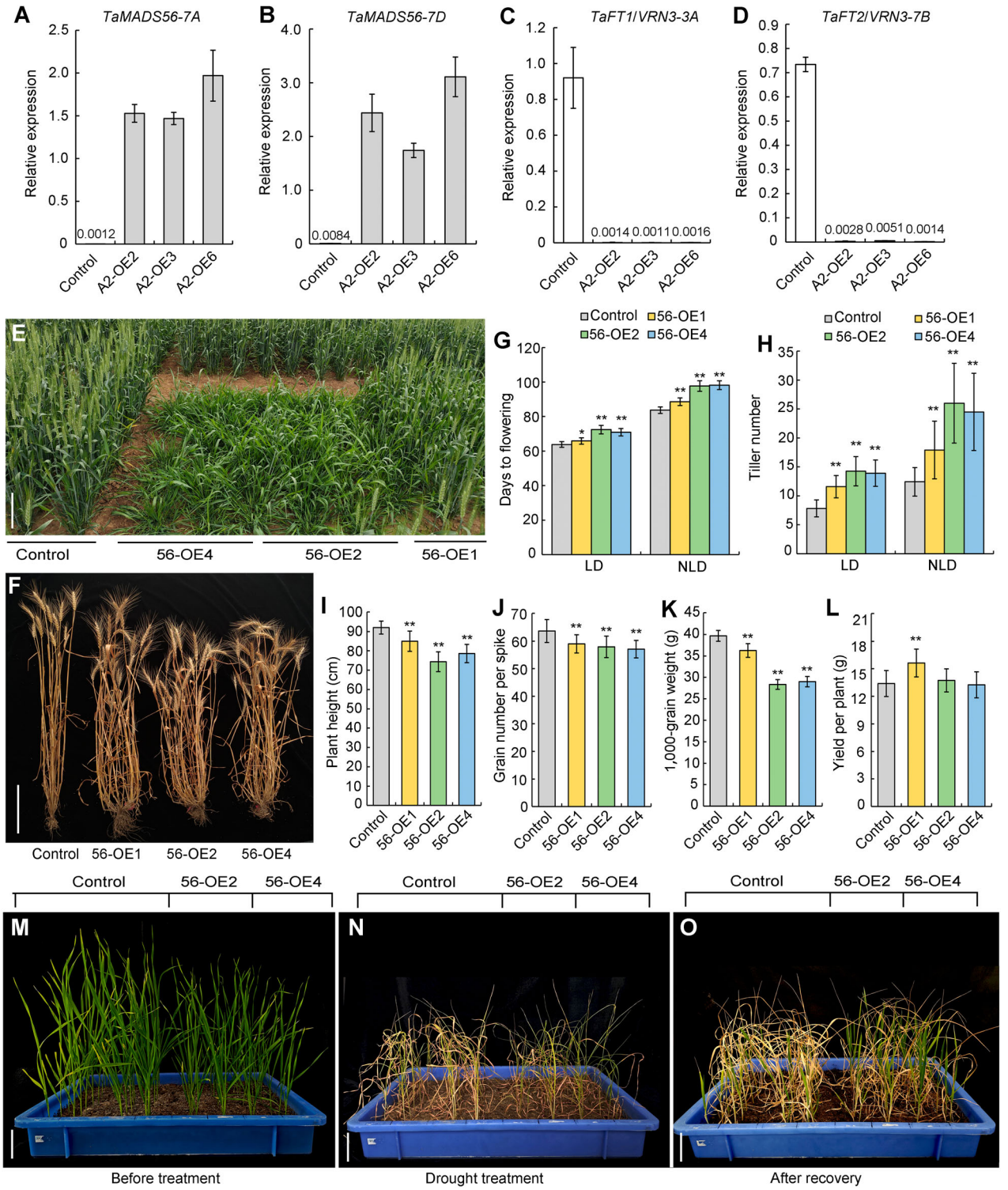

Figure 4. Overexpression of *TaMADS56* enhances vegetative growth and post-drought recovery in wheat

(A–D) RT-qPCR analysis of *TaMADS56-7A* **(A)**, *TaMADS56-7D* **(B)**, *TaFT1* **(C)**, and *TaFT2* **(D)** in control and *TaERF109A2*-OE (A2-OE2, A2-OE3, and A2-OE6) plants. The *TaActin* gene was used as an internal control. The data represent the means ± *SD* of three independent biological replicates. **(E, F)** Comparison of *TaMADS56*-OE (56-OE1, 56-OE2, and 56-OE4) and control plant at the tillering stage **(E)** and maturity stage **(F)** under natural long-day (NLD) field conditions. **(G, H)** Flowering time **(G)** and tiller number **(H)** of control and *TaMADS56*-OE plants under NLD and long-day (LD) conditions (14 h light/10 h dark). **(I–L)** Plant height **(I)**, grain number per spike **(J)**, 1,000-grain weight **(K)**, and yield per plant **(L)** of control and *TaMADS56*-OE plants in the field. Data are shown as means ± *SD* ($n = 12$). Significant differences were determined by two-tailed Student's *t*-test ($0.01 < {}^{*}P < 0.05$, ${}^{**}P < 0.01$). **(M–O)** Phenotypes of control and *TaMADS56*-OE plants under normal growth **(M)**, drought stress **(N)**, and post-rehydration **(O)** conditions. Scale bar = 30 cm **(E)**, 20 cm **(F)**, and 8 cm **(M–O)**.

Genomes (KEGG) pathway analyses were performed to classify and characterize the biological functions of DEGs from RNA-seq data. DEGs associated with zeatin biosynthesis were significantly upregulated in *TaERF109A*-OE plants (Figure S16). Among these, *TaIPT8-5B* and *TaIPT8-5D*, two isopentenyltransferase genes encoding rate-limiting enzymes in CK biosynthesis, were upregulated in the RNA-seq data, a finding that was validated by RT-qPCR (Figure 5A). In contrast, *TaIPT3* and *TaIPT6* were downregulated in *TaERF109A2*-OE plants (Figure 5B).

To determine whether TaERF109A2 directly activates *TaIPT8s* by binding to their promoters, we analyzed the 2-kb upstream regulatory regions of *TaIPT8-5B* and *TaIPT8-5D* and identified two GCC-box motifs (5′-AGCCGCC-3′) in each promoter (Figure 5C). Electrophoretic mobility shift assays (EMSA) were conducted using biotin-labeled probes encompassing these core sequences. As shown in Figure 5D, the recombinant TaERF109A2 protein induced a mobility shift in the labeled probes, and this binding was competitively reduced by excess unlabeled fragments, confirming specific *in vitro* interactions. Transient luciferase (LUC) reporter assays were performed using the *TaIPT8-5A*, *TaIPT8-5B*, and *TaIPT8-5D*. Co-expression with 35S:*TaERF109A2* significantly increased luciferase activity driven by the *TaIPT8-5B* and *TaIPT8-5D* promoters compared to the vector controls (Figure 5E, F).

Isopentenyladenine (iP)- and trans-zeatin (tZ)-type CKs are the dominant active CK species in plants, while the glucosylation pathway serves as a key mechanism for plants to prevent the overaccumulation of CKs (Chen et al., 2021). As *TaIPT8* expression levels increased in *TaERF109A2*-OE plants, the levels of iP- and tZ-type CKs, including their glucosylated forms, trans-zeatin 9-glucoside (tZ9G), and isopentenyladenine 9-glucoside (iP9G), were significantly elevated (Figure 6A). To confirm that *TaIPT8-5B* and *TaIPT8-5D* act as downstream targets of TaERF109, we generated

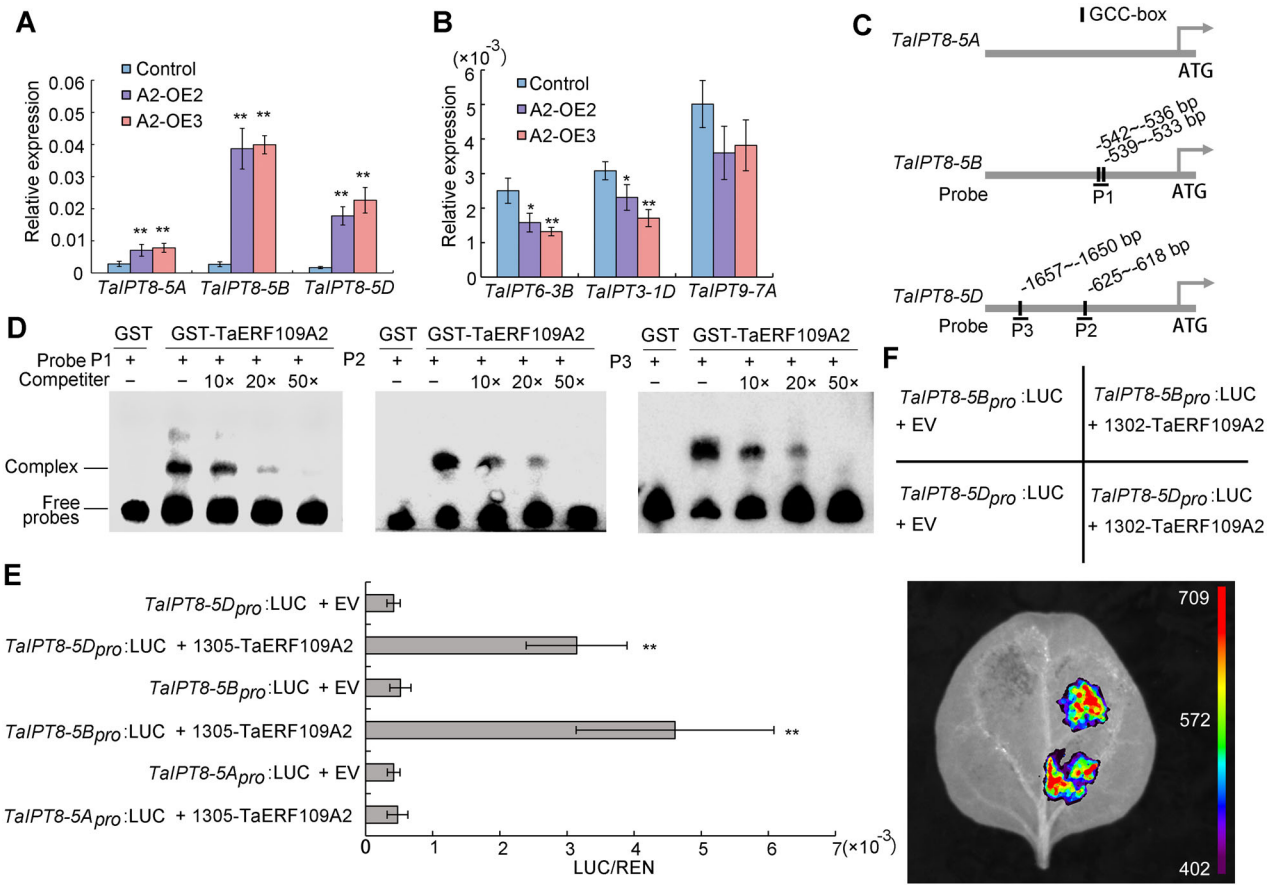

Figure 5. TaERF109A2 directly regulates *TaIPT8-5B/5D* expression

(A, B) RT-qPCR analysis of *TaIPT8* **(A)** and other *TaIPT* family genes **(B)** in control and *TaERF109A2*-OE (A2-OE2 and A2-OE3) plants. The *TaActin* gene was used as an internal control. The data represent the means ± *SD* of three independent biological replicates. **(C)** The schematic illustration of the locations of GCC-boxes cis-elements in the promoter of *TaIPT8-5A/5B/5D*. Probes P1, P2, and P3 span the predicted TaERF109A2 binding sites for the EMSA assays. **(D)** TaERF109A2-dependent mobility shifts were detected using EMSA. Biotin-labeled probes were incubated with maltose-binding protein (GST) or GST-TaERF109A2 proteins. Unlabeled probes were used as competitors. **(E, F)** The transcriptional activation of TaERF109A2 on the *TaIPT8* promoter was analyzed using luciferase reporter assays. Quantification of LUC activities in the leaves is shown in **(E)**. Asterisks indicate significant differences in the LUC/REN ratio between reporter constructs co-infiltrated with an empty vector (EV) and the 1305-TaERF109A2 vector. Values indicate means ± *SD* ($n = 8$). Significant differences were determined by a two-tailed Student's *t*-test (**$P < 0.01$).

TaIPT8-5A/5B/5D triple-mutant plants (*TaIPT8*-M1) and crossed them with the *TaERF109A2*-OE line (A2-OE3) by introducing the *Ubi-TaERF109A2* transgene into the mutant background (Figure 6B, C). Whereas A2-OE seedlings displayed a short root and shoot phenotype due to enhanced CK biosynthesis, the *TaIPT8*-M1 × A2-OE progeny exhibited a restored long root morphology similar to *TaIPT8*-M1 (Figure 6D–F). This genetic complementation shows that the TaERF109-mediated regulation of root length occurs primarily through TaIPT8-dependent CK biosynthesis.

TaERF109A2 overexpression enhances iron toxicity tolerance and drought tolerance via upregulation of *NAS* expression

To identify the molecular determinants and metabolic pathways underlying drought responses in *TaERF109A2*-OE plants, we performed gene ontology (GO) enrichment analysis and observed significant upregulation of transcripts associated with NA biosynthetic processes, NAS enzyme activity, heme binding, and iron ion binding (Figure S17A). Among these, 20 DEGs encoding NAS, the key enzyme catalyzing NA biosynthesis (Higuchi et al., 1999) were upregulated in *TaERF109A2*-OE lines (Figure S17B). As a non-proteinogenic amino acid, NA forms complexes with iron (II) and other divalent transition metal ions, such as Zn (II), Mn (II), and Cu (II). Its overaccumulation is linked to elevated intracellular metal ion concentrations. Consistent with this, measurements of NA and metal ion content in transgenic seedlings showed significantly higher levels of NA, Fe, Zn, Cu, and Mn in *TaERF109A2*-OE plants than in the control plants (Figure 7A–E). A recent study on *Arabidopsis* showed that AtERF109 regulates iron homeostasis by modulating iron-responsive genes, including *NAS4* (Yang et al., 2022), suggesting an orthologous role for its wheat homolog. To investigate whether increased NA biosynthesis in wheat could alleviate iron toxicity, we subjected

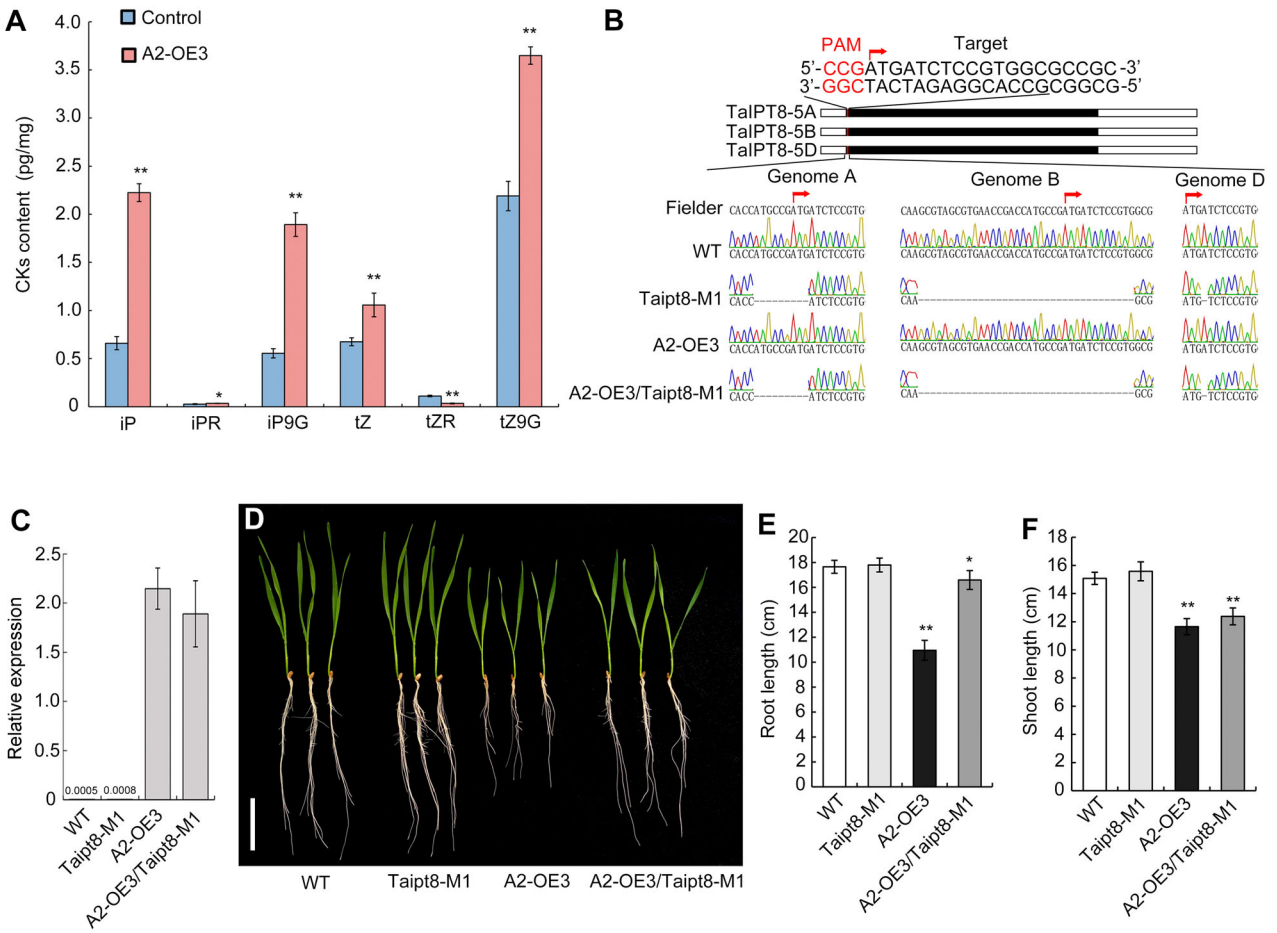

Figure 6. *TaERF109A2* acts upstream of *TaIPT8* to regulate cytokinin (CK) biosynthesis in wheat

(A) Cytokinin CK content in 30 d-old shoots of control and *TaERF109A2*-OE (A2-OE3) plants. Values are the means ± *SD* of three independent biological replicates. **(B)** Construct the *TaERF109A2* overexpression line (A2-OE3) in the *Taipt8*-M1 background. The sequences and sequencing chromatograms corresponding to the WT, *Taipt8*-M1, A2-OE3, and A2-OE3/*Taipt8*-M1 plants at target sites are shown; "–" indicates deletion of nucleotides; PAM motifs are highlighted in red; Red arrow indicates the start of translation. **(C)** RT-qPCR analysis of *TaERF109A2* in WT, *Taipt8*-M1, A2-OE3, and A2-OE3/*Taipt8*-M1 plants. The *TaActin* gene was used as an internal reference. The data represent the means ± *SD* of three independent biological replicates. **(D–F)** Root phenotypes **(D)**, root length **(E)**, and shoot length **(F)** of WT, *Taipt8*-M1, A2-OE3, and *Taipt8*-M1/A2-OE3 seedlings grown hydroponically in liquid culture. Scale bar = 5 cm **(D)**. Data are shown as means ± *SD* ($n = 8$). Significant differences were determined by two-tailed Student's *t*-test ($0.01 < {}^{*}P < 0.05$, ${}^{**}P < 0.01$).

TaERF109A2-OE and control seedlings to hydroponic cultures with 0, 20, 500, and 1,000 μM FeEDTA. Under normal iron conditions (20 μM FeEDTA), *TaERF109A2*-OE seedlings showed fewer adventitious roots and shorter primary roots and shoots compared to the controls. However, when exposed to high FeEDTA concentrations (500 and 1,000 μM), the control seedlings exhibited more pronounced inhibition of shoot and root growth. Notably, *TaERF109A2*-OE maintained comparable root architecture (length and adventitious root number) to controls under iron stress, while its shoot length was even longer than that of the controls (Figure 7F–I).

Previous studies have shown that NAS-mediated NA accumulation significantly enhances drought tolerance in rice. To elucidate *NAS* gene functions in wheat responses to iron

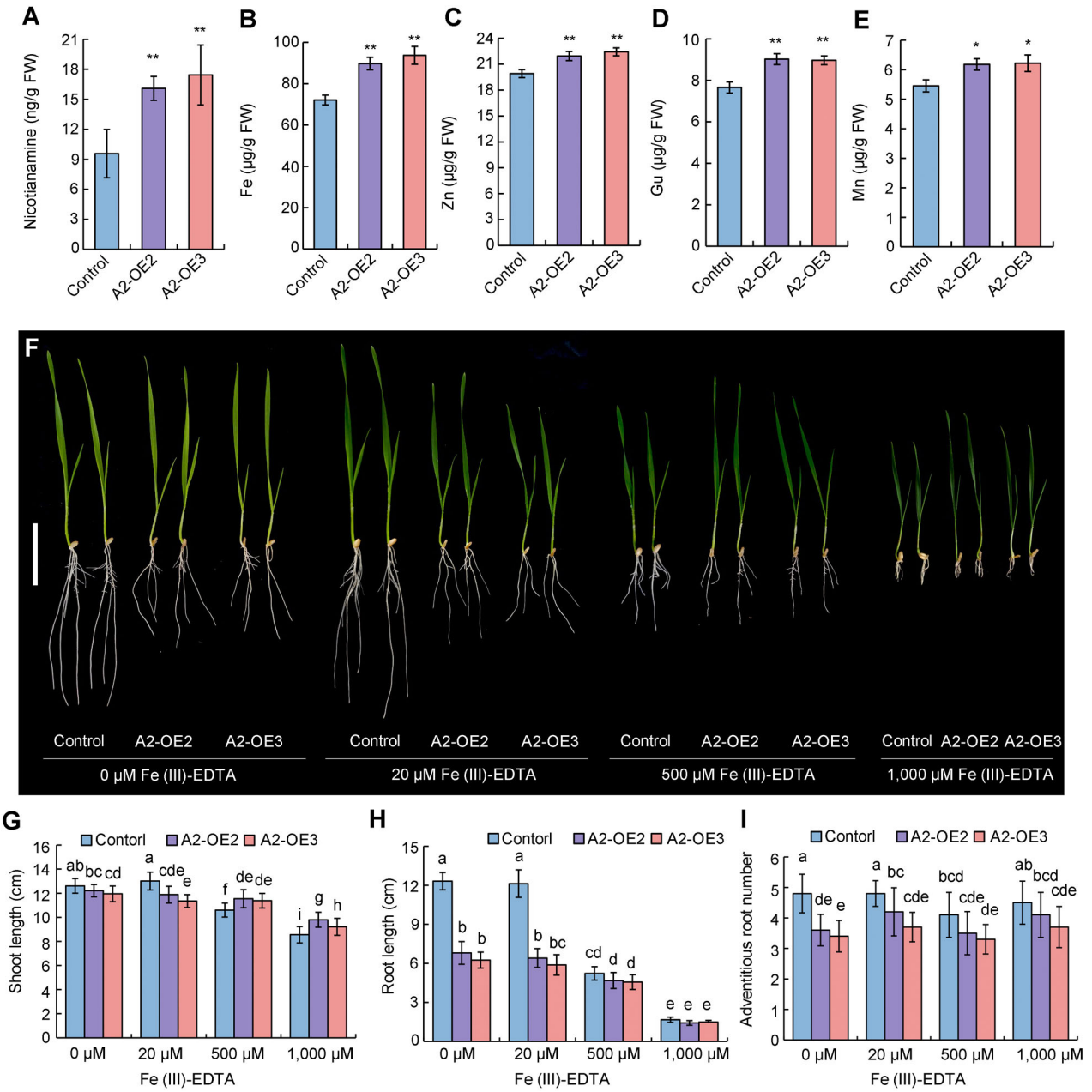

Figure 7. Overexpression of *TaERF109A2* enhanced nicotianamine (NA) biosynthesis and iron toxicity tolerance in wheat seedlings

(A–E) Quantification of nicotianamine NA and metal ion concentrations in shoots of control and *TaERF109A2*-OE (A2-OE2 and A2-OE3) plants. The data represent the means ± *SD* of three independent biological replications. Significant differences were determined by two-tailed Student's *t*-test ($0.01 < {}^{*}P < 0.05$, ${}^{**}P < 0.01$). **(F)** Phenotypic comparison of control and *TaERF109A2*-OE (A2-OE2 and A2-OE3) seedlings grown hydroponically in nutrient solutions with varying Fe concentrations (0, 20, 500, 1,000 μM) for 7 d. Scale bar = 4 cm. (**G–I**) Shoot length **(G)**, root length **(H)**, and adventitious root number **(I)** of control and *TaERF109A2*-OE (A2-OE2 and A2-OE3) seedlings grown hydroponically with different Fe concentrations. Data are shown as means ± *SD* ($n = 10$). Different letters above bar graphs indicate significance between groups at $P < 0.05$, according to Tukey's test.

toxicity and drought stress, we generated wheat overexpression lines of *TaNAS6B* (TraesCS6B02G425200), the most highly upregulated *NAS* gene in *TaERF109A2*-OE plants (Data S3). Hydroponic assays with 20, 500, and 1,000 μM FeEDTA revealed that *TaNAS6B*-OE lines had similar root lengths to controls under high iron conditions, but markedly longer shoots (Figure 8A–D). We subsequently selected two *TaNAS6B*-OE lines (NAS-OE2 and NAS-OE3) with relatively high expression levels for drought stress experiments. The results confirmed that *TaNAS6B*-OE lines are comparable to control plants under normal conditions but exhibit greater tolerance to drought stress, characterized by significantly reduced leaf rolling and wilting (Figure 8E–H), as well as higher fresh and dry weights following rewatering (Figure 8I, J). These results indicate that *TaERF109A2* confers enhanced tolerance to both iron toxicity and drought stress by mediating NAS-catalyzed NA accumulation.

DISCUSSION

TDG often encodes proteins involved in abiotic and biotic stress responses and plays pivotal roles in plant evolution and adaptation to environmental changes (Lynch and Conery, 2000; Hanada et al., 2008). In diverse plant taxa, *ERF109* homologs are rapidly upregulated in response to phytohormones and abiotic stresses, functioning in drought, salt, and cold tolerance pathways. We identified 10 *TaERF109* homologous genes in hexaploid wheat, seven of which were significantly induced by both drought and cytokinin treatments (Figures 1B, S3A). Functional analyses showed that *TaERF109A2* overexpression enhanced post-drought recovery rates and drought tolerance. Meanwhile, *Taerf109s* mutants had stunted growth and reduced grain yield under drought (Figures 2F–H, 3A–L). This confirmed that TaERF109 is a positive regulator of drought tolerance and resilience in wheat. Tandem replication events of a gene family are common across species and tend to be functionally conserved. Only ~10% of mammalian tandem arrays are species-specific, compared to > 20% in non-mammals (Pan and Zhang, 2008). Such lineage-specific duplications often drive the evolution of adaptive traits, enabling species to thrive in a niche environment (Yu et al., 2014). The genome of hexaploid wheat is composed of three subgenomes (Marcussen et al., 2014), each derived from a distinct diploid progenitor species. In these diploid ancestors, the *ERF109* gene exists as 2–4 tandem duplicates, which eventually leads to 9–10 copies in different hexaploid wheat accessions (Figure S7). Phylogenetic and microcollinearity analysis of publicly available genomes showed that *ERF109* tandem duplication events occurred exclusively in Triticeae (Figures S6, S7). The evolutionary retention of *ERF109* tandem copies in Triticeae crops may have facilitated their enhanced tolerance to recurrent abiotic stress through functional diversification or dosage effects.

Also designated as Redox-Responsive Transcription Factor 1 (RRTF1), ERF109 orchestrates diverse physiological and biochemical processes, including salt tolerance (Bahieldin et al., 2016), drought (Yu et al., 2017), cold (Wang et al., 2019), acclimation to high light intensity (Vogel et al., 2014), maintenance of redox (Khandelwal et al., 2008; Matsuo et al., 2015) and iron homeostasis (Yang et al., 2022), maintenance of root stem cells (Kong et al., 2018), and lateral root formation (Cai et al., 2014). Although phylogenetic analysis showed that *TaERF109* homologs in wheat were most closely related to those in barley and *A. tauschii*, their functions in wheat remain unclear. Given their low basal expression and membership in tandem-arrayed gene families, functional characterization was achieved through overexpression studies. *TaERF109A2*-OE seedlings showed enhanced tiller production under both control and post-rehydration conditions, deepening our understanding of their rapid drought recovery mechanisms (Figure 2A–I).

TaMADS56-7D expression was upregulated over 1,195-fold in *TaERF109A2*-OE plants (Figure 4B). *TaMADS56-7D*-OE lines recapitulated the key phenotypes of *TaERF109A2*-OE plants, including delayed flowering, increased tiller number, and improved drought recovery (Figure 4E–O). This suggests that *TaMADS56* acts as a genetic downstream effector in the regulation of heading date and tillering. No GCC-box cis-elements were identified in the 2.5-kb upstream genomic region of *TaMADS56*. Given that *TaMADS56* genes contain large introns (29–40 kb) that may harbor enhancer elements or alternative promoters for spatial regulation, whether *TaMADS56* is a direct transcriptional target of TaERF109A2 requires further validation. Furthermore, a total of 14 upregulated transcription factors containing the GCC-box were identified in *TaERF109A2*-OE RNA-seq data (Table S3), suggesting that *TaERF109* homologs may additionally modulate *TaMADS56* gene expression indirectly by initiating a TaERF109-dependent transcriptional cascade.

TaMADS56 proteins are homologs of *Arabidopsis* SOC1. *SOC1*-like genes that regulate floral development and flowering time have been widely studied in many plant taxa. However, none of these genes have been implicated in the control of tiller or branch numbers. Some *AP1/FUL*-like MADS-box genes play crucial roles not only in flowering time and floral organ regulation, but also in tillering coordination in rice. Transgenic rice lines overexpressing *OsMADS14*, *OsMADS15*, and *OsMADS18* flowered early, inhibited axillary bud growth, and reduced tiller numbers. Meanwhile, *OsMADS18* knockout mutants produced more tillers than the WT (Lu et al., 2012; Yin et al., 2019). In this study, *TaMADS56* overexpression lines exhibited accelerated tillering at the seedling stage. However, the expression levels of *TaMADS18* and *TaMADS15* were significantly suppressed at this stage in both the control and *TaMADS56*-OE lines (Figure S14C–D). *TaMADS15* and *TaMADS18* may only be involved in the TaMADS56-mediated regulation of the heading stage. Meanwhile, the molecular mechanism by which *TaMADS56* regulates wheat tillering requires further validation.

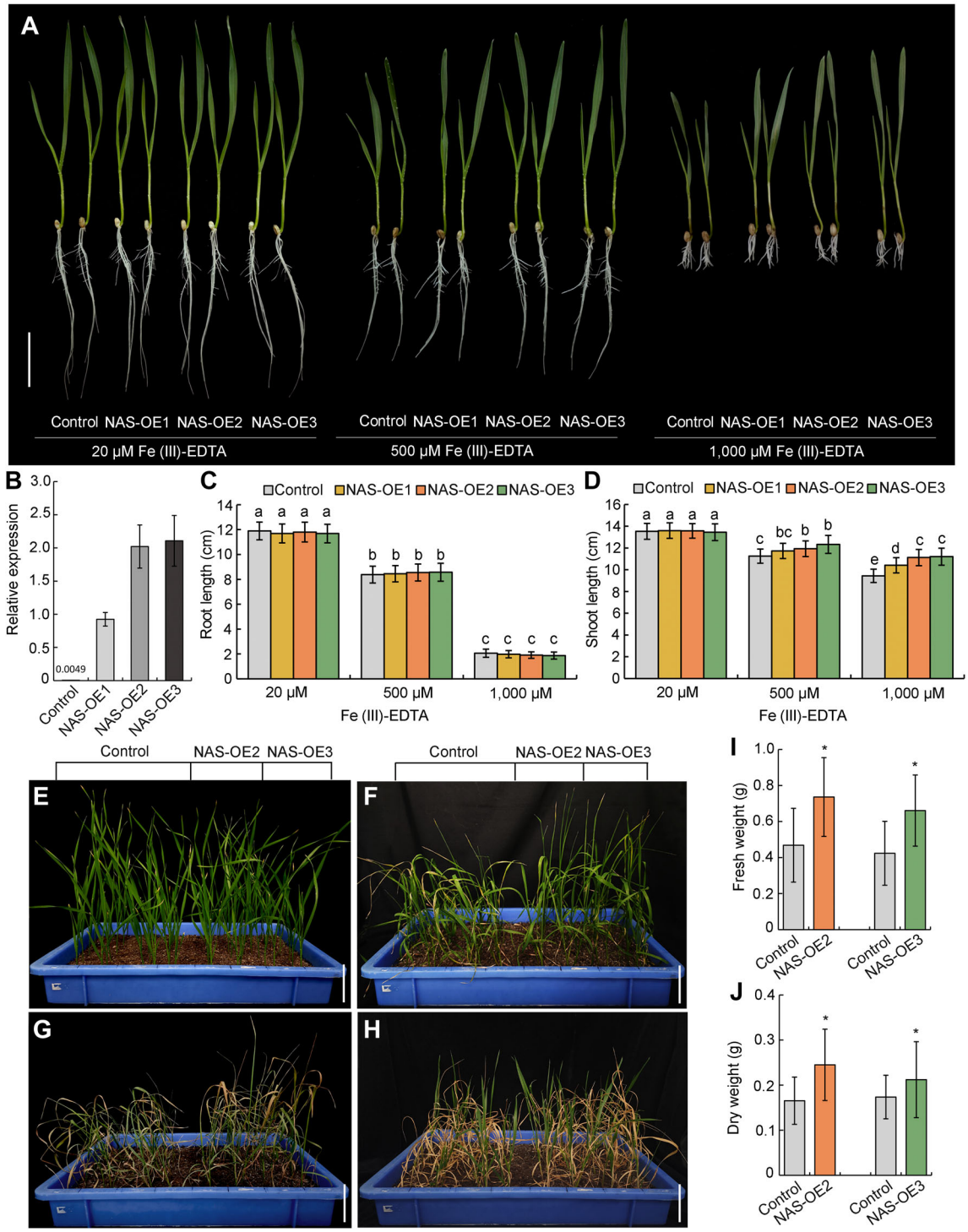

Figure 8. Overexpression of *TaNAS6B* enhanced iron toxicity and drought tolerance in wheat seedlings

(A) Phenotypic comparison of control and *TaNAS6B*-OE (NAS-OE1, NAS-OE2, and NAS-OE3) seedlings grown hydroponically in nutrient solutions with varying Fe concentrations (20, 500, 1,000 μM) for 10 d. Scale bar = 4 cm. **(B)** RT-qPCR analysis of *TaNAS6B* in control and *TaNAS6B*-OE (NAS-OE1, NAS-OE2, and NAS-OE3) plants. The *TaActin* gene was used as an internal control. The data represent the means ± *SD* of three independent biological replicates. **(C, D)** Root length **(C)** and shoot length **(D)** of control and *TaNAS6B*-OE (NAS-OE1, NAS-OE2, and NAS-OE3) seedlings grown hydroponically with different Fe concentrations. Data are shown as means ± *SD* ($n = 10$). Different letters above bar graphs indicate significance between groups at $P < 0.05$, according to Tukey's test. **(E–H)** *TaNAS6B*-OE (NAS-OE2 and NAS-OE3) and control seedlings grown for 14 d **(E)** were subjected to drought stress for 7 d **(F)** or 14 d **(G)** and then allowed to recover for 12 d **(H)**. Scale bar = 8 cm. **(I, J)** Fresh weight **(I)** and dry weight **(J)** of control and *TaNAS6B*-OE (NAS-OE2 and NAS-OE3) plants after water recovery. Data are shown as means ± *SD* from three independent replicates ($n = 9$). Significant differences were determined by a two-tailed Student's *t*-test (*$P < 0.05$).

Hydroponic experiments showed that root length was unaffected in *TaMADS56*-OE plants, indicating that increased *TaMADS56* expression could not explain the root growth inhibition observed in *TaERF109A2*-OE lines (Figure S12C). Phytohormones are major endogenous regulators of root growth. In Arabidopsis, AtERF109 mediates the crosstalk between jasmonic acid and auxin during lateral root formation. Meanwhile, in rice, OsERF109 negatively affects ethylene biosynthesis and drought tolerance (Cai et al., 2014; Yu et al., 2017). In wheat, the CK-responsive transcription factor TaERF109A2 directly binds to the GCC-box motifs in the promoters of *TaIPT8B* and *TaIPT8D*, thereby rapidly regulating CK biosynthesis (Figures 5D, 6A). *TaIPT8* expression spiked within 0.5–1 h of drought treatment before returning to basal levels, mirroring the kinetics of *TaERF109A2* induction (Wang et al., 2023). Root elongation was completely arrested in *TaERF109A2*-OE plants, and the short root phenotype of *TaERF109A2*-OE plants was largely rescued in *TaIPT8* knockout backgrounds (Figure 6D–F). These findings suggested that *TaERF109A2* acts upstream of *TaIPT8* to modulate CK biosynthesis during the early stages of drought stress, uncoupling the root growth-regulatory role of TaMADS56-mediated tillering pathways.

RNA-seq analysis identified 20 *NAS* genes that were upregulated in *TaERF109A2*-OE plants (Figure S17B). As key enzymes in NA biosynthesis, NAS proteins catalyze the production of these non-proteinogenic amino acids, which act as endogenous chelators of divalent metal ions to help maintain cellular ion homeostasis in plants. The chelation of Fe^{2+} by NA reduces its oxidative reactivity, mitigating Fe^{2}-induced cytotoxicity (Schuler et al., 2012). Consistent with previous reports in *Arabidopsis*, rice, and wheat (Ergen et al., 2009; Shaik and Ramakrishna, 2013), *NAS* expression was upregulated under drought conditions. In rice, OsNAC6-mediated *NAS* upregulation increases NA biosynthesis, promoting sequestration of excess Fe^{2+} and suppressing hydroxyl radical production to enhance drought resistance (Lee et al., 2017). Similarly, elevated *NAS* expression in *TaERF109A2*-OE plants was correlated with increased NA content, which was associated with improved tolerance to both high iron concentrations and drought stress in wheat (Figures 7F–H, 8A–J). These findings suggest that TaERF109A2 may mitigate drought-induced oxidative stress in wheat by rapidly upregulating NAS-dependent NA accumulation, which in turn buffers metal ion toxicity and maintains the redox balance under water-limited conditions.

Tandemly duplicated *TaERF109* gene family members function as molecular switches to coordinate stress responses and developmental programs in wheat by integrating hormonal signaling and metabolite biosynthesis to balance growth and stress resilience (Figure 9). These findings deepen our understanding of the functional diversification of duplicated genes in polyploid crops and provide valuable genetic resources to enhance drought tolerance in wheat breeding programs.

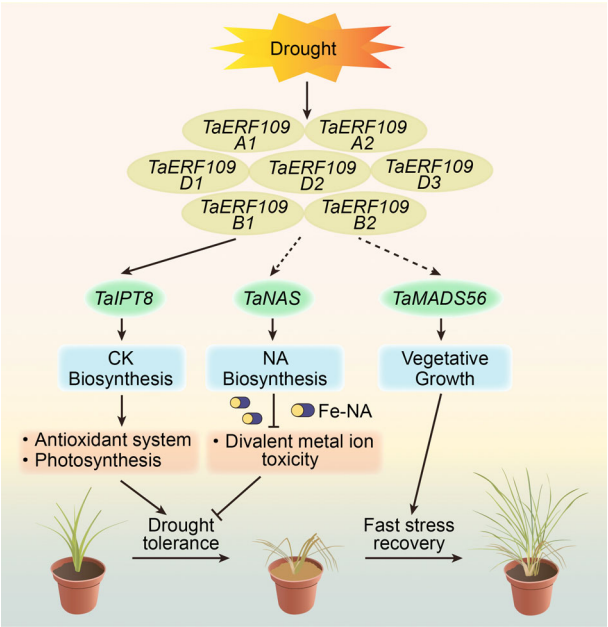

Figure 9. A proposed model illustrating *TaERF109* homologs regulating drought tolerance and water recovery in wheat
When subjected to drought stress, the expression levels of seven *TaERF109* genes, *TaERF109A1*, *TaERF109A2*, *TaERF109D1*, *TaERF109D2*, *TaERF109D3*, *TaERF109B1*, and *TaERF109B2,* are rapidly induced. These genes enhance wheat drought tolerance by upregulating *TaIPT8* and *TaNAS* expression to promote CK and NA synthesis. Additionally, they improve plant recovery ability after drought rewatering by upregulating *TaMADS56* expression. Solid lines indicate direct regulation and dashed lines indicate indirect regulation. This figure was created using Adobe Illustrator (Adobe Inc., San Jose, CA, USA).

MATERIALS AND METHODS

Construction of overexpression and CRISPR/Cas9 gene editing vectors

To generate *Taerf109s* mutants, two sgRNA target sequences were designed within the conserved exon regions of nine *TaERF109* homologs: TraesCS1A02G370400, TraesCS1A02G370600, TraesCS1A02G370700, TraesCS1B02G389700, TraesCS1B02G389900, TraesCS1D02G376500, TraesCS1D02G376600, TraesCS1D02G376700, and TraesCS1D02G376800, using CRISPR-P 2.0 (http://crispr.hzau.edu.cn/CRISPR2/). The wheat TaU3 promoter was amplified from the pCBC-MT1T2 vector using primers incorporating the designed sgRNAs (Table S4) and then cloned into the pBUE411 vector via Golden Gate assembly with BsaI digestion and T4 DNA ligase (TransGen Biotech). The transgenic wheat (cv. 'Fielder') was generated via Agrobacterium-mediated transformation (Wang et al., 2017). Genomic DNA of transgenic wheat plants was extracted from leaves, and the regions spanning the two target sites were amplified using nine *TaERF109-specific* PCR primers, purified, and sequenced.

To generate wheat overexpression lines, the full-length coding regions (CDS) of *TaERF109A2*, *TaERF109D4*, *TaMADS56-7D,* and *TaNAS6B* were amplified from wild-type

cDNA using DNA polymerase KOD FX (Toyobo, Osaka, Japan). They were then cloned into the pMWB110 vector (Liu et al., 2020) using an In-Fusion Advantage PCR cloning kit (Clontech Laboratories, Takara). The recombinant plasmids were transformed into the spring wheat cultivar "Fielder" using Agrobacterium-mediated gene transformation (Wang et al., 2017). All primer sequences used in this study are listed in Table S4.

Protein domain and motif prediction of *TaERF109* genes

To investigate cis-acting elements in the promoter regions of 10 *TaERF109* genes, 2 kb upstream promoter sequences relative to the translational start site were retrieved for each gene from Ensembl Plants (http://plants.ensembl.org). These promoter sequences were then submitted to the PlantCARE database (http://bioinformatics.psb.ugent.be/webtools/plantcare/html/) for analysis (Lescot 2002). After data standardization and organization, cis-acting elements in the promoters were visualized using TBtools-II (Chen et al., 2023). For analyzing the conserved and divergent characteristics of TaERF109 protein domains, domain annotation files of the 10 genes were acquired from NCBI (https://www.ncbi.nlm.nih.gov/), followed by visual comparative analysis of the protein domains via TBtools-II (Chen et al., 2023).

Growth conditions and drought treatments

For the phenotypic observation, control and transgenic wheat were planted in plastic pots filled with peat soil under controlled phytotron conditions: 14/10 h light/dark photoperiod, 70% relative humidity, and 25°C/22°C Day/Night temperatures. To ensure uniform soil moisture across genotypes, the control and transgenic seeds were germinated and grown in the same pots (1:1 ratio). For drought tolerance analysis, three-week-old seedlings were subjected to progressive soil drying by withholding irrigation. When differences in leaf wilting (approximately 14 d, soil water content $< 8\%$ w/w) were observed between transgenic and control plants, all plants were rehydrated. Phenotypic recovery was scored 7 d after rehydration. All drought treatments were repeated three times independently. For RNA in situ hybridization and subcellular localization analysis, plants were grown in a hydroponic growth box containing Hoagland solution in controlled greenhouses.

RNA extraction and RT-qPCR analyses

Three-week-old seedlings grown under well-watered conditions were subjected to rapid dehydration by placement on dry filter paper. Leaf samples were harvested at 0, 5, 15, 30, 60, 120, 240, and 480 min post-treatment and immediately snap-frozen in liquid nitrogen and stored at −80°C before RNA extraction. Total RNA was extracted from the tissues using a FastPure Universal Plant Total RNA Isolation Kit (Vazyme Biotech, Nanjing, China) according to the manufacturer's instructions. The first strand of cDNA was synthesized using the HiScript III 1st Strand cDNA Synthesis Kit (Vazyme Biotech, Nanjing, China). RT-qPCR was performed using gene-specific primers (Table S4) and Taq Pro Universal SYBR qPCR Master Mix (Vazyme Biotech, Nanjing, China) on an ABI 7500 Fast Real-Time PCR system (Applied Biosystems, Foster City, CA, USA). Wheat *TaActin* was used as an internal control. PCR was performed in triplicate for each sample, with three independent biological replicates.

RNA *in situ* hybridization

RNA *in situ* hybridization was performed as previously described (Bradley et al., 1993). A 345 bp *TaERF109A2* specific coding region was subcloned into the pGEM-T Easy vector (Promega, Madison, Wisconsin, USA) and used as a template to generate both antisense (for target detection) and sense (negative control) RNA probes. Shoot apexes of WT wheat seedlings at the 3rd leaf stage before and after 0.5 h drought treatments were excised and immediately fixed in RNase-free formalin-acetic acid-alcohol (FAA) solution (50% ethanol, 5% acetic acid, 3.7% formaldehyde in DEPC-treated water) at 4°C for 24 h. They were then embedded in paraffin (Leica Microsystems, Germany). Serial longitudinal sections (8 μM thickness) were prepared with a Leica RM2245 rotary microtome. Digoxigenin-labeled RNA probes were prepared using the DIG Northern Starter Kit (Roche, Mannheim, Germany) according to the manufacturer's instructions. After hybridization, the labeled probe was detected using an anti-DIG antibody coupled to alkaline phosphatase and 4-nitroblue tetrazolium chloride/5-bromo-4-chloro-3-indolyl-phosphate (NBT/BCIP; Roche, Mannheim, Germany). Slides were observed under a bright field using a Leica DMR microscope.

Subcellular localization analysis

The CDS of *TaERF109A2* was amplified using *Spe*I/*Xba*I restriction sites and cloned into the pAN580 vector (CaMV 35S promoter-driven) in-frame with the N-terminus of green fluorescent protein (GFP), generating the 35S: *TaERF109A2-GFP* construct. Wheat mesophyll protoplasts were isolated from two-week-old seedlings (cv. 'Fielder'). The TaERF109A2-GFP fusion protein and the nuclear marker EHD4-mCherry (Gao et al., 2013) were co-transformed into wheat leaf protoplasts for instantaneous expression using the polyethylene glycol 4000-mediated method. A Leica TCS-SP4 confocal microscope was used for fluorescence analysis.

Transient luciferase assay in tobacco

The 1.5 kb promoter regions of *TaIPT8-5A* (TraesCS 5A02G460000), *TaIPT8-5B* (TraesCS5B02G469600), and *TaIPT8-5D* (TraesCS5D02G471100) were amplified from wheat genomic DNA and cloned into the pGreenII-0800-LUC reporter vector containing Renilla luciferase (*REN*) as an internal control. The CDS of wheat *TaERF109A2* was cloned into pCAMBIA 1305.1, replacing the *GUS* reporter gene with the CaMV 35S. The constructed effector and reporter plasmids were co-transfected into four-week-old *Nicotiana benthamiana* leaves via *Agrobacterium*-mediated gene

transformation. Infiltrated plants were incubated at 23°C in the dark for 12 h, followed by 24 h under a 16/8 h light/dark cycle. LUC and REN activities were detected separately using a dual-luciferase reporter assay system (Promega, Madison, Wisconsin, USA). Data were collected as the LUC/REN ratios. All transient expression experiments were repeated three times.

Preparation of fusion protein and EMSA assay

The CDS of *TaERF109A2* was cloned into a pGEX-4T-1 vector. GST-TaERF109A2 and GST fusion proteins were induced in *Escherichia coli* Transseta (DE3) with 0.1 mM isopropyl-β-d-thiogalactoside at 20°C for 16 h and purified using glutathione-Sepharose 4B beads (Pharmacia, GE Healthcare, Sweden) according to the manufacturer's protocol. The biotin-labeled probes were heated at 95°C for 10 min, annealed at room temperature, and diluted to final concentrations of 50 fmol/μL. EMSA was performed using the Light-Shift Chemiluminescent EMSA Kit (Thermo Fisher Scientific, Waltham, MA, USA); 500 ng purified fusion protein GST-TaERF109A2 or GST protein and 100 fmol probe were added to the reaction mixture, and the binding reaction was performed at 25°C for 30 min. DNA was isolated on a 6.5% polyacrylamide gel and transferred onto nylon membranes (Millipore, Milford, MA, USA). Signals were detected using the Immobilon Western horseradish peroxidase substrate (Millipore, Milford, MA, USA).

Measurement of endogenous CK

Fresh third-leaf samples of WT and transgenic seedlings were harvested 30 d after germination, immediately frozen in liquid nitrogen, ground to powder, and stored at −80°C until analysis. CK concentrations were extracted and measured at the National Centre for Plant Gene Research (Beijing), Institute of Genetics and Developmental Biology, Chinese Academy of Sciences (Beijing, China), according to a previously described method (Du et al., 2017).

Analysis of NA and metal levels

Liquid chromatography (LC) with tandem mass spectrometry analysis was performed using an ultra-performance liquid chromatography (UPLC) system coupled with a triple quadrupole mass spectrometer (EXPEC 5210, PuYu Technology Development Co., Ltd., China). LC separation was performed using a BEH C18 column (1.7 μM, 100 × 2.1 mm; Waters, UK), with mobile phase A (0.1% formic acid in water) and B (methanol). The gradient was initially set to 20% B, which was increased to 80% B within 5 min. NA was detected in multiple reaction monitoring mode with transitions, and the transitions were as follows: 304 → 185, 304 → 114. Three biological replicates were analyzed for each treatment group.

For metals content determination, leaf samples from each replicate were dried (at 70°C for 48 h) and digested in nitric (HNO_3) and perchloric acids ($HClO_4$). The total concentrations of Fe, Zn, Gu, and Mn in the digests were determined using an inductively coupled plasma mass spectroscopy (ICP-MS) instrument (Agilent Technologies 7700x, Santa Clara, CA, USA) as previously described (Banakar et al., 2017).

RNA sequencing and analysis

Total RNA was extracted from the second top leaves of control and *TaERF109A2*-OE3 plants at 50 DAF. Libraries were constructed using the VAHTS Universal V6 RNA-seq Library Prep Kit (Vazyme Biotech, Nanjing, China) according to the manufacturer's instructions. Transcriptome sequencing and analyses were conducted by OE Biotech Co., Ltd. (Shanghai, China). The libraries were sequenced on an Illumina NovaSeq. 6000 platform, and 150 bp paired-end reads were generated. The clean data were filtered from the raw data using FASTP (Chen et al., 2018) and aligned to the *Triticum aestivum* reference genome using HISAT2 (Kim et al., 2015). The FPKM (Roberts et al., 2011) of each gene was calculated, and the read counts of each gene were obtained using HTSeq-count (Anders et al., 2015). Differentially expressed genes were screened using DESeq. 2 (Love et al., 2014), where genes that met the thresholds of fold-change ≥ 2 and *P*-value ≤ 0.05 were defined as DEGs.

Based on the hypergeometric distribution and GO and KEGG pathways, enrichment analysis of DEGs was performed to screen for significantly enriched terms using R (v 3.2.0). All raw reads were submitted to the National Center for Biotechnology Information (NCBI).

Data availability statement

RNA-seq data from this article can be found in the GenBank data libraries under accession numbers: SRP071191, SRR31770812, SRR31770813, SRR31770814, SRR3177 0815, SRR31770816, and SRR31770817.

ACKNOWLEDGEMENTS

We would like to thank Dr. Jinfang Chu from the Institute of Genetics and Developmental Biology, Chinese Academy of Sciences, for her assistance in the determination of CK content. This research was financially supported by the National Key R&D Program of China (2022YFF1001600), National Natural Science Foundation of China (32472197), and Major Project on Agricultural Bio-breeding of China (2023ZD04026).

CONFLICTS OF INTEREST

The authors declare no conflicts of interest.

AUTHOR CONTRIBUTIONS

J.C. and Y.M. coordinated the project, conceived and designed experiments, and edited the manuscript. S.Z., W.L., C.W., Y.Z., and J.C. performed most of the molecular, genetic, and biochemical experiments. Y.G. did software analysis. C.W. performed a wheat transformation assay. J.C. wrote the original draft. M.C. provided analytical tools and

managed reagents. Z.X. and Y.M. acquired funds. All authors read and approved the content.

Edited by: Yingyin Yao, China Agricultural University, China

Received Aug. 14, 2025; **Accepted** Jan. 26, 2026; **Published** Feb. 26, 2026

OO: OnlineOpen

REFERENCES

Abid, M., Ali, S., Qi, L.K., Zahoor, R., Tian, Z., Jiang, D., Snider, J.L., and Dai, T. (2018). Physiological and biochemical changes during drought and recovery periods at tillering and jointing stages in wheat (*Triticum aestivum* L.). Sci. Rep. **8:** 4615.

Anders, S., Pyl, P.T., and Huber, W. (2015). HTSeq—A Python framework to work with high-throughput sequencing data. Bioinformatics **31:** 166–169.

Bahieldin, A., Atef, A., Edris, S., Gadalla, N.O., Ali, H.M., Hassan, S.M., Al-Kordy, M.A., Ramadan, A.M., Makki, R.M., Al-Hajar, A.S.M., et al. (2016). Ethylene responsive transcription factor *ERF109* retards PCD and improves salt tolerance in plant. BMC Plant Biol. **16:** 216.

Banakar, R., Alvarez Fernández, Á., Abadía, J., Capell, T., and Christou, P. (2017). The expression of heterologous Fe (III) phytosiderophore transporter *HvYS1* in rice increases Fe uptake, translocation and seed loading and excludes heavy metals by selective Fe transport. Plant Biotechnol. J. **15:** 423–432.

Borner, R., Kampmann, G., Chandler, J., Gleißner, R., Wisman, E., Apel, K., and Melzer, S. (2000). A MADS domain gene involved in the transition to flowering in Arabidopsis. Plant J. **24:** 591–599.

Bradley, D., Carpenter, R., Sommer, H., Hartley, N., and Coen, E. (1993). Complementary floral homeotic phenotypes result from opposite orientations of a transposon at the plena locus of antirrhinum. Cell **72:** 85–95.

Cai, X., Xu, P., Zhao, P., Liu, R., Yu, L., and Xiang, C. (2014). Arabidopsis *ERF109* mediates cross-talk between jasmonic acid and auxin biosynthesis during lateral root formation. Nat. Commun. **5:** 5833.

Chen, C., Wu, Y., Li, J., Wang, X., Zeng, Z., Xu, J., Liu, Y., Feng, J., Chen, H., He, Y., et al. (2023). TBtools-II: A "one for all, all for one" bioinformatics platform for biological big-data mining. Mol. Plant **16:** 1733–1742.

Chen, S., Zhou, Y., Chen, Y., and Gu, J. (2018). fastp: An ultra-fast all-in-one FASTQ preprocessor. Bioinformatics **34:** i884–i890.

Chen, Y., Song, W., Xie, X., Wang, Z., Guan, P., Peng, H., Jiao, Y., Ni, Z., Sun, Q., and Guo, W. (2020). A collinearity-incorporating homology inference strategy for connecting emerging assemblies in the Triticeae tribe as a pilot practice in the plant pangenomic era. Mol. Plant **13:** 1694–1708.

Chen, L., Zhao, J., Song, J., and Jameson, P.E. (2021). Cytokinin glucosyl transferases, key regulators of cytokinin homeostasis, have potential value for wheat improvement. Plant Biotechnol. J. **19:** 878–896.

Du, Y., Liu, L., Li, M., Fang, S., Shen, X., Chu, J., and Zhang, Z. (2017). *UNBRANCHED3* regulates branching by modulating cytokinin biosynthesis and signaling in maize and rice. New Phytol. **214:** 721–733.

Ergen, N.Z., Thimmapuram, J., Bohnert, H.J., and Budak, H. (2009). Transcriptome pathways unique to dehydration tolerant relatives of modern wheat. Funct. Integr. Genomics **9:** 377–396.

Flagel, L.E., and Wendel, J.F. (2009). Gene duplication and evolutionary novelty in plants. New Phytol. **183:** 557–564.

Gao, H., Zheng, X.-M., Fei, G., Chen, J., Jin, M., Ren, Y., Wu, W., Zhou, K., Sheng, P., Zhou, F., et al. (2013). *Ehd4* encodes a novel and oryza-genus-specific regulator of photoperiodic flowering in rice. PLoS Genet. **9:** e1003281.

Glover, N.M., Daron, J., Pingault, L., Vandepoele, K., Paux, E., Feuillet, C., and Choulet, F. (2015). Small-scale gene duplications played a major role in the recent evolution of wheat chromosome 3B. Genome Biol. **16:** 188.

Hanada, K., Zou, C., Lehti-Shiu, M.D., Shinozaki, K., and Shiu, S.-H. (2008). Importance of lineage-specific expansion of plant tandem duplicates in the adaptive response to environmental stimuli. Plant Physiol. **148:** 993–1003.

Hao, C., Jiao, C., Hou, J., Li, T., Liu, H., Wang, Y., Zheng, J., Liu, H., Bi, Z., Xu, F., et al. (2020). Resequencing of 145 landmark cultivars reveals asymmetric sub-genome selection and strong founder genotype effects on wheat breeding in China. Mol. Plant **13:** 1733–1751.

Higuchi, K., Suzuki, K., Nakanishi, H., Yamaguchi, H., Nishizawa, N.-K., and Mori, S. (1999). Cloning of nicotianamine synthase genes, novel genes involved in the biosynthesis of phytosiderophores. Plant Physiol. **119:** 471–480.

Hoenicka, H., Nowitzki, O., Hanelt, D., and Fladung, M. (2008). Heterologous overexpression of the birch *FRUITFULL*-like MADS-box gene *BpMADS4* prevents normal senescence and winter dormancy in *Populus tremula* L. Planta **227:** 1001–1011.

Hussain, J., Khaliq, T., Ahmad, A., Akhter, J., and Asseng, S. (2018). Wheat responses to climate change and its adaptations: A focus on arid and semi-arid environment. Int. J. Environ. Res. **12:** 117–126.

Jin, Y., Yang, H., Wei, Z., Ma, H., and Ge, X. (2013). Rice male development under drought stress: Phenotypic changes and stage-dependent transcriptomic reprogramming. Mol. Plant **6:** 1630–1645.

Jung, H., Chung, P.J., Park, S., Redillas, M.C.F.R., Kim, Y.S., Suh, J., and Kim, J. (2017). Overexpression of *OsERF48* causes regulation of *OsCML16*, a calmodulin-like protein gene that enhances root growth and drought tolerance. Plant Biotechnol. J. **15:** 1295–1308.

Kane, J., Freeling, M., and Lyons, E. (2010). The evolution of a high copy gene array in Arabidopsis. J. Mol. Evol. **70:** 531–544.

Khandelwal, A., Elvitigala, T., Ghosh, B., and Quatrano, R.S. (2008). Arabidopsis transcriptome reveals control circuits regulating redox homeostasis and the role of an AP2 transcription factor. Plant Physiol. **148:** 2050–2058.

Kim, D., Langmead, B., and Salzberg, S.L. (2015). HISAT: A fast spliced aligner with low memory requirements. Nat. Methods **12:** 357–360.

Kimura, Y., Aoki, S., Ando, E., Kitatsuji, A., Watanabe, A., Ohnishi, M., Takahashi, K., Inoue, S., Nakamichi, N., Tamada, Y., et al. (2015). A flowering integrator, *SOC1*, affects stomatal opening in *Arabidopsis thaliana*. Plant Cell Physiol. **56:** 640–649.

KIRSCHBAUM, M.U.F. (1988). Recovery of photosynthesis from water stress in *Eucalyptus pauciflora*—A process in two stages. Plant Cell Environ. **11:** 685–694.

Kong, X., Tian, H., Yu, Q., Zhang, F., Wang, R., Gao, S., Xu, W., Liu, J., Shani, E., Fu, C., et al. (2018). *PHB3* maintains root stem cell niche identity through ROS-responsive AP2/ERF transcription factors in Arabidopsis. Cell Rep. **22:** 1350–1363.

Kutter, C., Schöb, H., Stadler, M., Meins, F., and Si-Ammour, A. (2007). MicroRNA-mediated regulation of stomatal development in Arabidopsis. Plant Cell **19:** 2417–2429.

Le, D.T., Nishiyama, R., Watanabe, Y., Vankova, R., Tanaka, M., Seki, M., Ham, L.H., Yamaguchi-Shinozaki, K., Shinozaki, K., and Tran, L.-S.P. (2012). Identification and expression analysis of cytokinin metabolic genes in soybean under normal and drought conditions in relation to cytokinin levels. PLoS One **7:** e42411.

Lee, J., and Lee, I. (2010). Regulation and function of SOC1, a flowering pathway integrator. J. Exp. Bot. **61:** 2247–2254.

Lee, D., Chung, P.J., Jeong, J.S., Jang, G., Bang, S.W., Jung, H., Kim, Y.S., Ha, S., Choi, Y., Do, E., et al. (2017). The rice *OsNAC6* transcription factor orchestrates multiple molecular mechanisms involving root structural adaptions and nicotianamine biosynthesis for drought tolerance. Plant Biotechnol. J. **15:** 754–764

Lescot, M. (2002). PlantCARE, a database of plant cis-acting regulatory elements and a portal to tools for in silico analysis of promoter sequences. Nucleic Acids Res. **30:** 325–327.

Li, J., Li, Y., Yin, Z., Jiang, J., Zhang, M., Guo, X., Ye, Z., Zhao, Y., Xiong, H., Zhang, Z., et al. (2017a). *OsASR5* enhances drought tolerance through a stomatal closure pathway associated with ABA and H_2O_2 signalling in rice. Plant Biotechnol. J. **15:** 183–196.

Li, N., Huang, B., Tang, N., Jian, W., Zou, J., Chen, J., Cao, H., Habib, S., Dong, X., Wei, W., et al. (2017b). The MADS-Box gene *SlMBP21* regulates sepal size mediated by ethylene and auxin in tomato. Plant Cell Physiol. **58:** 2241–2256.

Liu, Z., Lv, Y., Zhang, M., Liu, Y., Kong, L., Zou, M., Lu, G., Cao, J., and Yu, X. (2013). Identification, expression, and comparative genomic analysis of the *IPT* and *CKX* gene families in Chinese cabbage (*Brassica rapa* ssp. *pekinensis*). BMC Genomics **14:** 594.

Liu, H., Wang, K., Jia, Z., Gong, Q., Lin, Z., Du, L., Pei, X., and Ye, X. (2020). Efficient induction of haploid plants in wheat by editing of *TaMTL* using an optimized Agrobacterium-mediated CRISPR system. J. Exp. Bot. **71:** 1337–1349.

Love, M.I., Huber, W., and Anders, S. (2014). Moderated estimation of fold change and dispersion for RNA-seq data with DESeq. 2. Genome Biol. **15:** 550.

Lu, S.-J., Wei, H., Wang, Y., Wang, H.-M., Yang, R.-F., Zhang, X.-B., and Tu, J.-M. (2012). Overexpression of a transcription factor *OsMADS15* modifies plant architecture and flowering time in rice (*Oryza sativa* L.). Plant Mol. Biol. Report **30:** 1461–1469.

Lynch, M., and Conery, J.S. (2000). The evolutionary fate and consequences of duplicate genes. Science **290:** 1151–1155.

Ma, Q., and Liu, Y. (2009). Expression of isopentenyl transferase gene (*ipt*) in leaf and stem delayed leaf senescence without affecting root growth. Plant Cell Rep. **28:** 1759–1765.

Macková, H., Hronková, M., Dobrá, J., Turečková, V., Novák, O., Lubovská, Z., Motyka, V., Haisel, D., Hájek, T., Prášil, I.T., et al. (2013). Enhanced drought and heat stress tolerance of tobacco plants with ectopically enhanced cytokinin oxidase/dehydrogenase gene expression. J. Exp. Bot. **64:** 2805–2815.

Magar, M.M., Liu, H., and Yan, G. (2022). Genome-wide analysis of AP2/ERF superfamily genes in contrasting wheat genotypes reveals heat stress-related candidate genes. Front. Plant Sci. **13:** 853086.

Marcussen, T., Sandve, S.R., Heier, L., Spannagl, M., Pfeifer, M., Jakobsen, K.S., Wulff, B., Steuernagel, B., Mayer, K.F.X., Olsen, O.A., et al. (2014). Ancient hybridizations among the ancestral genomes of bread wheat. Science **345:** 1250092.

Matsubara, K., Shimamura, K., Kodama, H., Kokubun, H., Watanabe, H., Basualdo, I.L., and Ando, T. (2008). Green corolla segments in a wild Petunia species caused by a mutation in *FBP2*, a SEPALLATA-like MADS box gene. Planta **228:** 401–409.

Matsuo, M., Johnson, J.M., Hieno, A., Tokizawa, M., Nomoto, M., Tada, Y., Godfrey, R., Obokata, J., Sherameti, I., Yamamoto, Y.Y., et al. (2015). High REDOX RESPONSIVE TRANSCRIPTION FACTOR1 levels result in accumulation of reactive oxygen species in *Arabidopsis thaliana* shoots and roots. Mol. Plant **8:** 1253–1273.

Melzer, S., Lens, F., Gennen, J., Vanneste, S., Rohde, A., and Beeckman, T. (2008). Flowering-time genes modulate meristem determinacy and growth form in *Arabidopsis thaliana*. Nat. Genet. **40:** 1489–1492.

Merewitz, E.B., Gianfagna, T., and Huang, B. (2011). Photosynthesis, water use, and root viability under water stress as affected by expression of SAG12-*ipt* controlling cytokinin synthesis in *Agrostis stolonifera*. J. Exp. Bot. **62:** 383–395.

Nakano, T., Suzuki, K., Fujimura, T., and Shinshi, H. (2006). Genome-wide analysis of the *ERF* gene family in Arabidopsis and Rice. Plant Physiol. **140:** 411–432.

Nishiyama, R., Watanabe, Y., Fujita, Y., Le, D.T., Kojima, M., Werner, T., Vankova, R., Yamaguchi-Shinozaki, K., Shinozaki, K., Kakimoto, T., et al. (2011). Analysis of cytokinin mutants and regulation of cytokinin metabolic genes reveals important regulatory roles of cytokinins in drought, salt and abscisic acid responses, and abscisic acid biosynthesis. Plant Cell **23:** 2169–2183.

Pan, D., and Zhang, L. (2008). Tandemly Arrayed Genes in Vertebrate Genomes. Comp. Funct. Genomics **2008:** 1–11.

Panchy, N., Lehti-Shiu, M., and Shiu, S.-H. (2016). Evolution of gene duplication in plants. Plant Physiol. **171:** 2294–2316.

Pei, Z.-M., Murata, Y., Benning, G., Thomine, S., Klüsener, B., Allen, G.J., Grill, E., and Schroeder, J.I. (2000). Calcium channels activated by hydrogen peroxide mediate abscisic acid signalling in guard cells. Nature **406:** 731–734.

Peleg, Z., Reguera, M., Tumimbang, E., Walia, H., and Blumwald, E. (2011). Cytokinin-mediated source/sink modifications improve drought tolerance and increase grain yield in rice under water-stress. Plant Biotechnol. J. **9:** 747–758.

Prerostova, S., Dobrev, P.I., Gaudinova, A., Knirsch, V., Körber, N., Pieruschka, R., Fiorani, F., Brzobohatý, B., černý, M., Spichal, L., et al. (2018). Cytokinins: Their impact on molecular and growth responses to drought stress and recovery in Arabidopsis. Front. Plant Sci. **9:** 655.

Qin, H., Gu, Q., Zhang, J., Sun, L., Kuppu, S., Zhang, Y., Burow, M., Payton, P., Blumwald, E., and Zhang, H. (2011). Regulated expression of an *Isopentenyltransferase* gene (*IPT*) in peanut significantly improves drought tolerance and increases yield under field conditions. Plant Cell Physiol. **52:** 1904–1914.

Reddy, A.R., Chaitanya, K.V., and Vivekanandan, M. (2004). Drought-induced responses of photosynthesis and antioxidant metabolism in higher plants. J. Plant Physiol. **161:** 1189–1202.

Rivero, R.M., Kojima, M., Gepstein, A., Sakakibara, H., Mittler, R., Gepstein, S., and Blumwald, E. (2007). Delayed leaf senescence induces extreme drought tolerance in a flowering plant. Proc. Natl. Acad. Sci. U. S. A. **104:** 19631–19636.

Roberts, A., Trapnell, C., Donaghey, J., Rinn, J.L., and Pachter, L. (2011). Improving RNA-Seq expression estimates by correcting for fragment bias. Genome Biol. **12:** R22.

Sakuma, Y., Liu, Q., Dubouzet, J.G., Abe, H., Shinozaki, K., and Yamaguchi-Shinozaki, K. (2002). DNA-binding specificity of the ERF/AP2 Domain of Arabidopsis *DREBs*, transcription factors involved in dehydration- and cold-inducible gene expression. Biochem. Biophys. Res. Commun. **290:** 998–1009.

Sato, K., Abe, F., Mascher, M., Haberer, G., Gundlach, H., Spannagl, M., Shirasawa, K., and Isobe, S. (2021). Chromosome-scale genome assembly of the transformation-amenable common wheat cultivar 'Fielder'. DNA Res. **28:** dsab008.

Schuler, M., Rellán-Álvarez, R., Fink-Straube, C., Abadía, J., and Bauer, P. (2012). Nicotianamine functions in the phloem-based transport of iron to sink organs, in pollen development and pollen tube growth in Arabidopsis. Plant Cell **24:** 2380–2400.

Shaik, R., and Ramakrishna, W. (2013). Genes and co-expression modules common to drought and bacterial stress responses in Arabidopsis and Rice. PLoS ONE **8:** e77261.

Tan, M., Li, G., Qi, S., Liu, X., Chen, X., Ma, J., Zhang, D., and Han, M. (2018). Identification and expression analysis of the *IPT* and *CKX* gene families during axillary bud outgrowth in apple (*Malus domestica* Borkh.). Gene **651:** 106–117.

Vogel, M.O., Moore, M., König, K., Pecher, P., Alsharafa, K., Lee, J., and Dietz, K.-J. (2014). Fast retrograde signaling in response to high light involves metabolite export, *MITOGEN-ACTIVATED PROTEIN KINASE*6, and AP2/ERF transcription factors in Arabidopsis. Plant Cell **26:** 1151–1165.

Wang, K., Liu, H., Du, L., and Ye, X. (2017). Generation of marker-free transgenic hexaploid wheat via an Agrobacterium-mediated co-

transformation strategy in commercial Chinese wheat varieties. Plant Biotechnol. J. **15:** 614–623.

Wang, M., Dai, W., Du, J., Ming, R., Dahro, B., and Liu, J. (2019). ERF109 of trifoliate orange (*Poncirus trifoliata* (L.) Raf.) contributes to cold tolerance by directly regulating expression of *Prx1* involved in antioxidative process. Plant Biotechnol. J. **17:** 1316–1332.

Wang, W., Wang, Z., Li, X., Ni, Z., Hu, Z., Xin, M., Peng, H., Yao, Y., Sun, Q., and Guo, W. (2020). SnpHub: An easy-to-set-up web server framework for exploring large-scale genomic variation data in the post-genomic era with applications in wheat. Gigascience **9:** giaa060.

Wang, N., Chen, J., Gao, Y., Zhou, Y., Chen, M., Xu, Z., Fang, Z., and Ma, Y. (2023). Genomic analysis of isopentenyltransferase genes and functional characterization of *TaIPT8* indicates positive effects of cytokinins on drought tolerance in wheat. Crop J. **11:** 46–56.

Werner, T., Nehnevajova, E., Köllmer, I., Novák, O., Strnad, M., Krämer, U., and Schmülling, T. (2011). Root-specific reduction of cytokinin causes enhanced root growth, drought tolerance, and leaf mineral enrichment in Arabidopsis and tobacco. Plant Cell **22:** 3905–3920.

Xu, Z., Chen, M., Li, L., and Ma, Y. (2011). Functions and application of the AP2/ERF transcription factor family in crop improvement. J. Integr. Plant Biol. **53:** 570–585.

Yang, Z., and Qin, F. (2023). The battle of crops against drought: Genetic dissection and improvement. J. Integr. Plant. Biol **65:** 496–525.

Yang, C.L., Huang, Y.T., Schmidt, W., Klein, P., Chan, M.T., and Pan, I.C. (2022). Ethylene response factor109 attunes immunity, photosynthesis, and iron homeostasis in Arabidopsis leaves. Front. Plant Sci. **13:** 841366.

Yin, X., Liu, X., Xu, B., Lu, P., Dong, T., Yang, D., Ye, T., Feng, Y.-Q., and Wu, Y. (2019). OsMADS18, a membrane-bound MADS-box transcription factor, modulates plant architecture and the abscisic acid response in rice. J. Exp. Bot. **70:** 3895–3909.

Yu, J., Tehrim, S., Zhang, F., Tong, C., Huang, J., Cheng, X., Dong, C., Zhou, Y., Qin, R., Hua, W., et al. (2014). Genome-wide comparative analysis of NBS-encoding genes between Brassica species and *Arabidopsis thaliana*. BMC Genomics **15:** 3.

Yu, Y., Yang, D., Zhou, S., Gu, J., Wang, F., Dong, J., and Huang, R. (2017). The ethylene response factor *OsERF109* negatively affects ethylene biosynthesis and drought tolerance in rice. Protoplasma **254:** 401–408.

Zhang, P., Wang, W., Zhang, G., Kaminek, M., Dobrev, P., Xu, J., and Gruissem, W. (2010). Senescence-inducible expression of isopentenyl transferase extends leaf life, increases drought stress resistance and alters cytokinin metabolism in Cassava. J. Integr. Plant Biol. **52:** 653–669.

Zhang, X., Lei, L., Lai, J., Zhao, H., and Song, W. (2018). Effects of drought stress and water recovery on physiological responses and gene expression in maize seedlings. BMC Plant Biol. **18:** 68.

SUPPORTING INFORMATION

Additional Supporting Information may be found online in the supporting information tab for this article: http://onlinelibrary.wiley.com/doi/10.1111/jipb.70196/suppinfo

Data S1. Tandemly repeated genes in DEGs of drought treatment
Data S2. Distribution of SNP genotypes in *TaERF109B2* regions across 145 wheat accessions
Data S3. *NAS* genes in DEGs of *TaERF109A2*-OE plants
Figure S1. Haplotype heatmap of *TaERF109B2*-associated chromosome regions in 145 wheat accessions
Figure S2. Conserved protein domain and promoter cis-acting element analysis of *TaERF109* homologs
Figure S3. Expression profiles of 10 *TaERF109* homologs in wheat under phytohormone and abiotic stress treatments
Figure S4. Expression profiles of 10 *TaERF109* homologs across different tissues of wheat
Figure S5. Subcellular localization and transcriptional activation analysis of TaERF109A2
Figure S6. Phylogenetic relationships of ERF109-like proteins
Figure S7. Microcollinearity analysis of tandemly duplicated *ERF109* homologs among the Triticeae tribe
Figure S8. Phenotypic characterization of the *TaERF109*-OE plants
Figure S9. Effects of drought stress on the content of proline, MDA, H_2O_2, and O_2^- in control and *TaERF109A2*-OE seedlings
Figure S10. Phenotypic characterization of the *Taerf109s* mutant
Figure S11. Effects of drought stress on the content of proline, MDA, H_2O_2, and O_2^- in WT and *Taerf109s* seedlings
Figure S12. Phenotypic characterization of the *TaMADS56*-OE plants
Figure S13. TaMADS56-7A/7D have no transcriptional activation activity in yeast
Figure S14. RT-qPCR analysis of flowering time regulatory genes in *TaMADS56*-OE plants
Figure S15. Fresh weight and dry weight of control and *TaMADS56*-OE plants after recovery
Figure S16. KEGG analysis of upregulated genes in *TaERF109A2*-OE plants
Figure S17. GO analysis reveals that overexpression of *TaERF109A2* enhances the expression of *NAS* genes
Table S1. Drought-induced *ERF109* genes among DEGs
Table S2. DEGs related to heading date in *TaERF109A2*-OE plants
Table S3. The positions of GCC-boxes in the promoters of differentially expressed transcription factors in *TaERF109A2*-OE plants
Table S4. Primers used in this study